

CHORUS

This is the accepted manuscript made available via CHORUS. The article has been published as:

Superconductivity versus bound-state formation in a two-band superconductor with small Fermi energy: Applications to Fe pnictides/chalcogenides and doped SrTiO₃

Andrey V. Chubukov, Ilya Eremin, and Dmitri V. Efremov

Phys. Rev. B **93**, 174516 — Published 25 May 2016

DOI: [10.1103/PhysRevB.93.174516](https://doi.org/10.1103/PhysRevB.93.174516)

Superconductivity vs bound state formation in a two-band superconductor with small Fermi energy – applications to Fe-pnictides/chalcogenides and doped SrTiO₃

Andrey V. Chubukov,¹ Ilya Eremin,² and Dmitri V. Efremov³

¹*Department of Physics, University of Minnesota, Minneapolis, Minnesota 55455, USA*

²*Institut für Theoretische Physik III, Ruhr-Universität Bochum, D-44801 Bochum, Germany*

³*Leibniz-Institut für Festkörper- und Werkstofforschung, D-01069 Dresden, Germany*

(Dated: March 24, 2016)

We analyze the interplay between superconductivity and the formation of bound pairs of fermions (BCS-BEC crossover) in a 2D model of interacting fermions with small Fermi energy E_F and weak attractive interaction, which extends to energies well above E_F . The 2D case is special because two-particle bound state forms at arbitrary weak interaction, and already at weak coupling one has to distinguish between bound state formation and superconductivity. We briefly review the situation in the one-band model and then consider two different two-band models – one with one hole band and one electron band and another with two hole or two electron bands. In each case we obtain the bound state energy $2E_0$ for two fermions in a vacuum and solve the set of coupled equations for the pairing gaps and the chemical potentials to obtain the onset temperature of the pairing, T_{ins} and the quasiparticle dispersion at $T = 0$. We then compute the superfluid stiffness $\rho_s(T = 0)$ and obtain the actual T_c . For definiteness, we set E_F in one band to be near zero and consider different ratios of E_0 and E_F in the other band. We show that, at $E_F \gg E_0$, the behavior of both two-band models is BCS-like in the sense that $T_c \approx T_{ins} \ll E_F$ and $\Delta \sim T_c$. At $E_F < E_0$, the two models behave differently: in the model with two hole/two electron bands, $T_{ins} \sim E_0 / \log \frac{E_0}{E_F}$, $\Delta \sim (E_0 E_F)^{1/2}$, and $T_c \sim E_F$, like in the one-band model. In between T_{ins} and T_c the system displays preformed pair behavior. In the model with one hole and one electron band, T_c remains of order T_{ins} , and both remain finite at $E_F = 0$ and of order E_0 . The preformed pair behavior still does exist in this model because T_c is numerically smaller than T_{ins} . For both models we re-express T_{ins} in terms of the fully renormalized two-particle scattering amplitude by extending to two-band case the method pioneered by Gorkov and Melik-Barkhudarov back in 1961. We apply our results for the model with a hole and an electron band to Fe-pnictides and Fe-chalcogenides in which superconducting gap has been detected on the bands which do not cross the Fermi level, and to FeSe, in which superconducting gap is comparable to the Fermi energy. We apply the results for the model with two electron bands to Nb-doped SrTiO₃ and argue that our theory explains rapid increase of T_c when both bands start crossing the Fermi level.

PACS numbers:

I. INTRODUCTION

The discovery of superconductivity in Fe-pnictides and later in Fe-chalcogenides opened up several new directions in the study of non-phononic mechanisms of electronic pairing in multi-band correlated electron systems^{1,2}. Two issues were brought about by recent angle-resolved photoemission and other experiments in Fe-based superconductors (FeSCs). First, in recent experiments on LiFe_{1-x}Co_xAs, Miao et al. observed³ a finite superconductive gap of 4 – 5meV on the hole band, which is located below the Fermi level, with the top of the band at 4-8meV away from E_F . Moreover, the gap on this hole band is larger than the gaps on electron bands, which cross the Fermi level. A similar observation has been reported for FeTe_{0.6}Se_{0.4}⁴, where superconductivity with the gap $\Delta = 1.3$ meV has been observed on an electron band which lies above the Fermi level, with the bottom of the band at 0.7 meV away from E_F . Second, recent photoemission measurements have demonstrated that in almost all Fe-based superconductors either electron or hole pockets are more tiny than previously thought and the corresponding dispersions ei-

ther barely cross the Fermi level or are fully located below or above it⁵. The "extreme" case in this respect is FeSe. In this material Fermi energies on *all* hole and electron pockets are small and are comparable to the magnitudes of the superconducting gaps (the reported E_F on different bands vary between 4 and 10 meV, while the gaps are 3-5meV^{6,7}).

The observation of a sizable superconducting gap on a band which does not cross the Fermi level was originally interpreted³ as the indication that the pairing in the FeSCs is a strong coupling phenomenon for which the pairing gap is not confined to the Fermi surface and develops at all momenta in the Brillouin zone. Later, however, the experiments were re-interpreted⁸ in a more conventional weak/moderate coupling scenario, as the consequence of the fact that in FeSCs the pairing interaction primarily "hopes" a pair of fermions with momenta \mathbf{k} and $-\mathbf{k}$ from one band to the other^{9,10}. In this situation, the gap on the band, which does not cross the Fermi level is determined by the density of states at E_F of the band which does cross the Fermi level. A solution of the coupled set of BCS gap equations for fermions in the two bands then shows that one crossing is sufficient to obtain

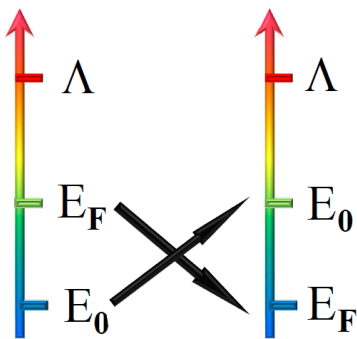


FIG. 1: Energy scales relevant to the interplay between the formation of bound pairs of fermions and true superconductivity in 2D Fermionic systems with weak attractive pairing interaction. Λ is the upper energy cutoff, E_F is the Fermi energy, and E_0 is the energy of a bound state of two fermions in a vacuum, i.e., at $\mu = 0$. At weak coupling, $E_0 \ll \Lambda$. We assume that E_F is also small and can be tuned by doping to be either larger or smaller than E_0 . We show that in one-band model and in two band model with two hole or two electron bands, the system displays BCS-like behavior at $E_F \gg E_0$ and BEC-like behavior at $E_F \ll E_0$. In the latter case, bound pairs develop at $T_{ins} \sim E_0 / \log \frac{E_0}{E_F}$ but the true superconductivity with full phase coherence develops at $T_c \sim E_F$. In between T_{ins} and T_c the system displays preformed pair behavior and the spectral function displays pseudogap behavior. In the two-band model with one hole and one electron pocket, T_{ins} and T_c also split when E_F gets smaller than E_0 , but both remain of order E_0 even when E_F vanishes. Still, superconducting T_c in this limit is several times smaller than T_{ins} , so there is a wide temperature range of preformed pair behavior.

BCS instability already at weak coupling⁸. This reasoning also naturally explains why the gap is larger on a band which does not cross the Fermi level.

The observation of superconductivity with $\Delta \sim E_F$ brought FeSCs into the orbit of long-standing discussion about the interplay between superconductivity and the formation of the bound pair of two fermions. This issue has been discussed in the condensed matter context^{11–27}, and also for optical lattices of ultracold atoms^{28,29}. The phenomenon in which bound pairs of fermions form at a higher T_{ins} and condense at a smaller T_c is often termed Bose-Einstein condensation (BEC) because the condensation of preformed pairs (i.e., the development of a macroscopic condensate) bears a direct analogy with BEC of bosons in a Bose gas. When Δ and T_c are much smaller than E_F , bound pairs and true superconductivity develop at almost the same temperature, i.e., $T_c \approx T_{ins}$. However, when E_F gets smaller, superconducting T_c is generally smaller than the onset temperature for bound state formation.

In the present communication, we discuss superconductivity vs bound state formation in 2D systems with weak attractive interaction U in the proper symmetry channel. (s^{+-} for the two-band model for FeSCs). We consider the situation when U remains energy indepen-

dent up to an energy Λ , which well exceeds E_F , see Fig.1. Elementary quantum mechanics shows that in 2D, two fermions with dispersion $k^2/(2m)$ form a bound state at arbitrary small attraction U , and the bound state energy is $2E_0$, where $E_0 \sim \Lambda e^{-2/\lambda}$, and $\lambda = mU/(2\pi)$ is a dimensionless coupling. We analyze the evolution of the system behavior and the interplay between T_c and T_{ins} by varying the ratio E_F/E_0 while keeping both E_F and E_0 well below Λ .

We briefly review BCS-BEC crossover in the one-band two-dimensional (2D) model and consider two different two-band models.

The first model, which we apply to FeSCs, consists of one hole and one electron band. We follow usual path and consider the case when the dominant pairing interaction is weak inter-band pair hopping interaction $U > 0$, in which case superconducting state has s^{+-} symmetry. We use the same computational procedure as in the studies of one-band model.^{11,13–15,20,26,27} Namely, we first obtain the bound state energy $2E_0$ for two fermions in a vacuum. Then we consider the actual system with a non-zero density of carriers in one of the bands $n = 2N_0E_F$, where N_0 is a 2D density of states at low energies, and solve the set of coupled equations for the chemical potential $\mu(T)$ and the pairing gaps at a finite T . The solution of the linearized gap equations yields the onset temperature of the pairing T_{ins} . The solution of non-linear gap equations at $T = 0$ yields the pairing gaps $\Delta_{h,e}$. We next use the values of $\Delta_{h,e}$ and μ at $T = 0$ as inputs and compute superfluid stiffness $\rho_s(T = 0)$. For definiteness, we consider the case when the chemical potential at $T = 0$ in the would be normal state is at the bottom of the electron band but crosses the hole band i.e., the Fermi energy is zero for the electron band but finite for the hole band.

We present the results in the two limits when E_F is either larger or smaller than E_0 and in the case when $E_F = E_0$. We show that in all cases the pairing gap develops on both bands and is larger on the electron band (the one which does not cross the Fermi level). This agrees qualitatively but not quantitatively with the results obtained previously within the conventional BCS theory^{8,30}, neglecting the renormalization of the chemical potential. We argue, however, that the renormalization of the chemical potential by both a finite temperature and a finite gap is not a small perturbation when the bare chemical potential touches the bottom of the electron band.

We argue that the onset temperature of the pairing, T_{ins} (the one obtained by solving the set of equations for the pairing gaps and the chemical potentials) evolves when E_F/E_0 changes and is of order $E_F^{1/3}E_0^{2/3}$ when $E_F \gg E_0$ and of order E_0 when $E_F \ll E_0$. We further argue that superconducting T_c is of order T_{ins} for arbitrary E_F/E_0 , but is numerically smaller than T_{ins} . The numerical smallness implies that there exists a finite range of temperatures between T_{ins} and T_c , where pairs are already formed but their phases are random and there is no superconductivity (the "preformed pairs" regime).

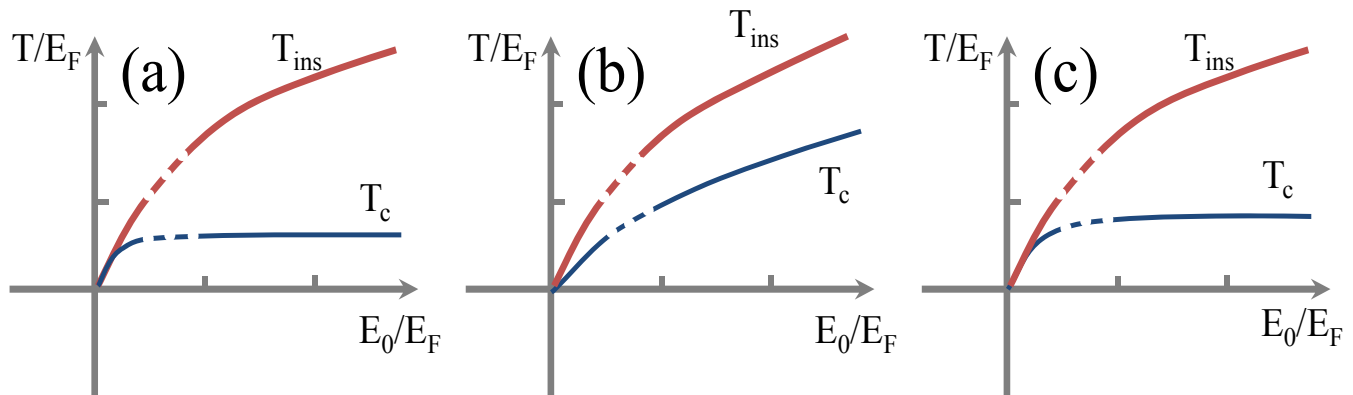


FIG. 2: The onset temperature T_{ins} for the bound state formation and the superconducting transition temperature T_c in the three models that we consider – the model with one electron band (a), with one electron band and one hole band (b), and with two electron bands (c). For all three cases we plot T_{ins} and T_c in units of E_F , as functions of E_0/E_F , where E_0 is the bound state energy for two free fermions in 2D. Dashed lines show T_c and T_{ins} in the intermediate regime $E_F/E_0 = O(1)$, where we didn't obtain the explicit formulas. The highest superconducting T_c at small E_F is for the model with one hole and one electron pockets. In this model both T_{ins} and T_c are of order E_0 at large E_0/E_F .

The emergence of the bound pairs at $T_{ins} > T_c$ and the existence of the preformed pairs regime is often associated with the crossover from BCS to BEC behavior. Such crossover has been studied in detail in the finite T analysis of 3D one-band model (Ref.¹⁵). The temperatures T_{ins} and T_c were found to differ strongly at $E_F \ll E_0$: $T_{ins} \sim E_0/\log \frac{E_0}{E_F} \gg E_F$, while $T_c \sim E_F$, i.e., the ratio T_c/T_{ins} vanishes at $E_F \rightarrow 0$. The behavior in the 2D case is quite similar (see below). In our two-band model the behavior is similar to the one-band model in that T_{ins} becomes parametrically larger than E_F at $E_F \ll E_0$, but differs in that T_c remains finite and of the same order as order T_{ins} even at $E_F \rightarrow 0$. The reason, as we argue below, is that the development of the pairing gap below T_{ins} reconstructs the fermionic dispersion and creates images, with opposite dispersion, of original hole and electron bands. This in turn gives rise to the shift of fermionic density from the filled hole band and empty electron band into these image bands. As a consequence, there appear new hole-like and electron-like bands with a finite density of carriers in each band, proportional to T_{ins} . Superconducting T_c scales with this density and is a fraction of T_{ins} . We show that preformed pair behavior still exists at $E_F \ll E_0$, but only because T_c , set by superconducting stiffness, is numerically smaller than T_{ins} .

We next consider the two-band model consisting of two electron bands. We again assume that the dominant pairing interaction is inter-band pair hopping $U > 0$ and that the chemical potential is at or near the bottom of one of the bands, but crosses the dispersion of the other band at some finite E_F . We show that, at $E_F \gg E_0$, the behavior of this model is nearly identical to that in the

model with a hole and an electron band. However, in the opposite limit $E_F \ll E_0$, the behavior of the model with two electron bands differs qualitatively from that of the model with a hole and an electron band and is quite similar to the behavior of the 2D one-band model in the BEC limit. Namely, $T_{ins} \sim E_0/\log \frac{E_0}{E_F}$ and $T_c \sim E_F$, such that the ratio T_c/T_{ins} vanishes at $E_F = 0$. The reason is that for the two bands with the same sign of dispersion, there are no free carriers at $E_F \rightarrow 0$, hence the pairing cannot create images of the original bands. Indeed, we show that in the model with two electron bands, the pairing gap Δ , which is responsible for the Fermi surface reconstruction, scales at $T = 0$ as $\sqrt{E_0 E_F}$ and vanishes at $E_F = 0$. The same behavior holds at $T = 0$ in the 2D one-band model.^{11,13}

Superconductivity in a system with two electron bands is realized experimentally in Nb-doped SrTiO₃ and, possibly, in heterostructures of LaAlO₃ and SrTiO₃ (see Refs.^{22,23,31} and references therein). The Fermi energy in one of the bands is finite already at zero doping and E_F is likely much larger than E_0 . The other electron band is above the chemical potential at zero doping, but the chemical potential μ moves up with doping and enters this band once it exceeds the critical value μ^* . The data indicate^{32,33} that, when this happens, T_c rapidly increases. To analyze this behavior we compute T_c for $\mu \neq \mu^*$. We show that T_c indeed increases when μ exceeds μ^* , and the rate of the increase is $(1 - \mu^*/\mu)(E_F/E_0)^{2/3}$, i.e., it is enhanced by a large ratio of E_F/E_0 .

We summarize our results for all three models in Fig. 2 and in the Table I.

	single-band	2 electron (hole) bands	1 electron and 1 hole bands
$E_F \gg E_0$	$T_{ins} \sim \sqrt{E_F E_0}$, $\mu(T_{ins}) \approx E_F$ $T_c \approx T_{ins}$, $\Delta = 2\sqrt{E_F E_0}$	$T_{ins} \sim E_F^{1/3} E_0^{2/3}$, $\mu_1(T_{ins}) \approx E_F$ $\mu_2(T_{ins}) \approx -0.5T_{ins}$, $T_c \approx T_{ins}$ $\Delta \approx 1.78E_F^{1/3} E_0^{2/3}$	$T_{ins} \sim E_F^{1/3} E_0^{2/3}$, $\mu_e(T_{ins}) \approx -0.5T_{ins}$ $\mu_h(T_{ins}) \approx E_F$, $T_c \approx T_{ins}$ $\Delta \approx 1.78E_F^{1/3} E_0^{2/3}$
$E_F \ll E_0$	$T_{ins} \approx E_0 / \log \frac{E_0}{E_F}$, $\mu(T_{ins}) \approx -E_0$ $T_c \sim E_F/8 \ll T_{ins}$, $\Delta = 2\sqrt{E_F E_0}$	$T_{ins} \sim 4.5E_0 / \log \frac{E_0}{E_F}$, $\mu_1(T_{ins}) \approx -2.3E_0$ $\mu_2(T_{ins}) \approx -2.3E_0$, $T_c \sim E_F/8 \ll T_{ins}$, $\Delta \approx \sqrt{2E_F E_0}$	$T_{ins} \sim 1.13E_0 \left(1 + 0.22 \frac{E_F}{E_0}\right)$, $\mu_h(T_{ins}) \approx 3E_F/2$, $\mu_e(T_{ins}) \approx -\frac{E_F}{2}$ $T_c \sim 0.22T_{ins}$, $\Delta = 1.76T_{ins}$
$E_F = E_0$	$T_{ins} = 1.09E_F$, $\mu(T_{ins}) = -0.09E_F$	$T_{ins} \sim 0.9E_F$, $\mu_1(T_{ins}) = 0.1E_F$ $\mu_2(T_{ins}) = -0.9E_F$, $\Delta = 1.4E_F$	$T_{ins} = 1.35E_F$, $\mu_e(T_{ins}) = -0.35E_F$ $\mu_h(T_{ins}) = 1.35E_F$, $T_c \sim 0.4E_F$ $\Delta = 2.4E_F$

TABLE I: The summary of the results for the onset temperature of the pairing, T_{ins} , the actual superconducting transition temperature, T_c , the gap magnitude at $T = 0$, Δ , and the chemical potentials, μ_i , for different ratios of the Fermi energy, E_F , and the bound state energy of two fermions in a vacuum, E_0 . For the one band model, superconductivity is an ordinary s -wave. For the two-band models, superconducting state has s^\pm - symmetry (different signs of the gaps on the two bands). The gap magnitudes on different bands are approximately the same in the two-band models, up to small corrections, but nevertheless the gap on the band which doesn't cross the chemical potential at $T \geq T_{ins}$ is larger than that on the other band, which crosses the chemical potential. The chemical potentials satisfy $\mu_h + \mu_e = E_F$ for the two band model with a hole and an electron band, and $\mu_1 - \mu_2 = E_F$ for the model with two electron bands.

Another goal of our work is to compare the analysis of BCS/BEC crossover with the approach put forward by Gorkov and Melik-Barkhudarov (GMB) back in 1961 (Refs.^{35,36}). GMB considered a one-band model with attractive Hubbard interaction U at weak coupling in $D=3$. They argued that superconductivity comes from fermions with energies not exceeding E_F , while all contributions to the pairing susceptibility from fermions with higher energies can be absorbed into the renormalization of the original 4-fermion interaction into quantum-mechanical scattering amplitude. GMB explicitly separated the Cooper logarithm (associated with the presence of a sharp Fermi surface at $E_F \neq 0$) from the renormalization of the interaction into the scattering amplitude and obtained $T_c = 0.277E_F e^{-\pi/(2|a|k_F)}$, where a is the s -wave scattering length. They argued that this is the right formula for comparison with the experimental data because the scattering length is the physically observable parameter, while the interaction U is not.

The GMB analysis does not include phase fluctuations, hence their instability temperature is the same as T_{ins} , re-expressed in terms of scattering amplitude. In the original GMB analysis (which we review in Sec. V below) $|a|k_F$ is assumed to be small, and no bound state develops. We extend GMB analysis to one-band and two-band models in 2D and will specifically consider the limit $E_F < E_0$. In this limit, the scattering amplitude diverges at the onset of bound state development at $T \sim E_0$ and changes sign at a smaller T . It is then *a-priori* unclear whether the onset temperature of the pairing, T_{ins} , can be expressed via the 2D scattering amplitude a_2 (dimensionless in 2D) with E_F in the prefactor, particularly given that the ratio T_{ins}/E_F tends to infinity when $E_F = 0$. We, however, show that GMB approach

remains valid even when $E_F < E_0$, and T_{ins} can be explicitly expressed via the exact 2D scattering amplitude, with E_F in the prefactor.

The paper is organized as follows. In Sec.II we review one-band 2D Fermi system with small E_F . We reproduce earlier results^{11,13,27} for the onset temperature for the pairing, T_{ins} , the pairing gap, the renormalized chemical potential, and the spin stiffness. We argue that superconducting T_c scales with E_F and vanishes when $E_F = 0$. In Sec. III we consider in detail the case of one hole and one electron bands, relevant to FeSCs. We show that in this model both T_{ins} and T_c remain finite even when neither bands crosses the Fermi level. The superconducting T_c is smaller than T_{ins} in this case, but the smallness is only numerical. In Sec. IV we consider the case of two hole/two electron pockets and show that that T_c remains non-zero as long as one of the band crosses Fermi level but vanishes when $E_F = 0$ for both bands. In Sec. V we review GMB formalism and then apply it first to 2D one-band model and then to 2D model with a hole and an electron band. In both cases we show that the instability temperature T_{GMB} is precisely T_{ins} , even when $E_F \rightarrow 0$. We present our conclusions in Sec. VI. Discussion of some technical details is moved into the Appendix.

In this work we only consider s -wave pairing (ordinary s -wave and s^{+-}) with angle-independent gap functions. The extension to the cases when the gaps are angle-dependent and have either symmetry-related or accidental nodes is straightforward, but requires separate, more involved calculations.

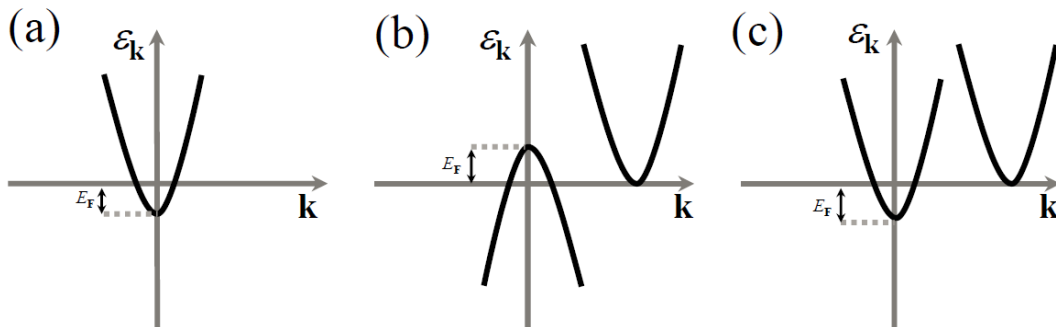


FIG. 3: The bare dispersion for the models considered in the present manuscript: (a) a one-band model of 2D fermions with the parabolic dispersion and a positive bare chemical potential (i.e., a non-zero E_F); (b) a two-band model with one hole and one electron band separated in the momentum space. For definiteness, we set the bare chemical potential such that it touches the bottom of the electron band and crosses the hole band at a finite distance from its top; (c) a two-band model with two electron bands separated in the momentum space. For definiteness we set the bare chemical potential to touch the bottom of one band and cross the other.

II. ONE-BAND MODEL

To set the stage for the analysis of the two-band model we first review pairing and superconductivity in the 2D one-band model. Consider a set of 2D fermions with the parabolic dispersion $\varepsilon_k = \frac{k^2}{2m}$ and chemical potential $\mu_0 = E_F$, see Fig.3(a). We assume that fermions get paired by a weak attractive pairing interaction $U(q, \Omega)$, which for simplicity we approximate as momentum and frequency independent U up to upper momentum cutoff q_{max} and corresponding frequency cutoff $\Lambda = q_{max}^2/(2m)$. For electron-phonon interaction Λ is of the order of Debye frequency. The actual dispersion does not have to be parabolic, however at weak coupling energies relevant for the pairing are much smaller than Λ and $\varepsilon_k = \frac{k^2}{2m}$ can be just viewed as the leading term in the expansion of the lattice dispersion in small momentum.

We introduce the dimensionless parameter

$$\lambda = N_0|U| = \frac{m|U|}{2\pi}, \quad (1)$$

where $N_0 = \frac{m}{2\pi}$ is the density of states in 2D. We assume that λ is small number. The conventional weak coupling BCS analysis is valid when the attraction is confined to energies much smaller than E_F , i.e., when $\Lambda \ll E_F$. We consider the opposite situation when E_F is much smaller than the cutoff energy Λ .

For two fermions with 2D k^2 dispersion in a vacuum (i.e., at $E_F = 0$), an arbitrary small attraction U gives rise to the formation of a bound state³⁷. The bound state energy at $T = 0$ is $2E_0$, where

$$E_0 = \Lambda e^{-\frac{2}{\lambda}} \quad (2)$$

The bound state develops at $T_0 = 1.13E_0$. The 2D

scattering amplitude $a_2 \propto 1/\log \frac{T_0}{T}$ diverges at $T = T_0$ and changes sign from negative at $T > T_0$ to positive at $T < T_0$. We consider the system at a non-zero E_F , i.e., at a finite density of fermions $n = mE_F/\pi$. We show that the system behavior is different at $E_F \gg E_0$ and at $E_F \ll E_0$.

A. The onset temperature of the pairing, the pairing gap and the renormalization of the chemical potential

The onset temperature of the pairing instability, T_{ins} (not necessary a true superconducting transition temperature) is obtained by introducing infinitesimal pairing vertex and dressing it by renormalizations to obtain the pairing susceptibility. The temperature T_{ins} is the one at which the pairing susceptibility diverges. To logarithmical accuracy, one needs to keep only ladder series of renormalizations in the particle-particle channel and neglect all renormalizations coming from particle-hole channel because the first contain series of $\lambda \log \frac{\Lambda}{T_{ins}}$ while the latter contain series in λ . We assume and then verify that in all cases that we consider, $T_{ins} \ll \Lambda$, hence $\log \frac{\Lambda}{T_{ins}}$ is a large factor. However, as we will see, the ratio of $\frac{T_{ins}}{E_F}$ is small only when $E_F \gg E_0$ and is actually large in the opposite limit $E_F \ll E_0$. Because temperature variation of the chemical potential $\mu(T)$ in the normal state holds in powers of T_{ins}/E_F , this variation generally cannot be neglected, i.e., the equation for the pairing vertex at $T = T_{ins}$ has to be combined with the equation for the chemical potential $\mu(T_{ins})$. The latter follows from the condition that the total number of fermions is con-

served.^{13,15} The two coupled equations are ($\mu = \mu(T_{ins})$)

$$\begin{aligned}
1 &= \frac{\lambda}{2} \int_0^\Lambda d\varepsilon \frac{\tanh \frac{\varepsilon - \mu}{2T_{ins}}}{\varepsilon - \mu} \\
&= \frac{\lambda}{2} \left(\int_0^\mu dx \frac{\tanh \frac{x}{2T_{ins}}}{x} + \int_0^\Lambda dx \frac{\tanh \frac{x}{2T_{ins}}}{x} \right) \\
E_F &= \int_0^\Lambda d\varepsilon \frac{1}{e^{(\varepsilon - \mu)/T_{ins}} + 1} = T_{ins} \log(1 + e^{\mu/T_{ins}})
\end{aligned} \tag{3}$$

At $E_F \gg E_0$, the solution of these equations yields

$$\begin{aligned}
T_{ins} &= 1.13(\lambda E_F)^{1/2} e^{-\frac{1}{\lambda}} \sim \sqrt{E_F E_0} \\
\mu(T_{ins}) &\approx E_F
\end{aligned} \tag{4}$$

In the opposite limit $E_F \ll E_0$ we obtain²⁷

$$\begin{aligned}
T_{ins} &= \frac{E_0}{\log \frac{E_0}{E_F}} \\
\mu(T_{ins}) &\approx -E_0
\end{aligned} \tag{5}$$

This behavior is rather similar to that in three-dimensional case.¹⁵ The behavior of T_{ins} and μ at intermediate $E_F \sim E_0$ can be easily obtained numerically.

For $E_F = E_0$, $T_{ins} \approx 1.09 E_F$ and $\mu(T_{ins}) \approx -0.09 E_F$. Note that at $E_F \gg E_0$, the instability temperature $T_{ins} \ll E_F$, while at $E_F \ll E_0$, $T_{ins} \gg E_F$ and $\mu(T_{ins})$ is negative.

The prefactor 1.13 in Eq. (4) is in fact obtained by going beyond logarithmical accuracy in the particle-particle channel. To get the correct prefactor one also needs to include fermionic self-energy to order λ and the renormalization of U by corrections from the particle-hole channel.^{35,36} These two renormalizations are not essential for our consideration and in the bulk of the text we neglect them. For completeness, however, we obtain the result for T_{ins} with the full prefactor in the Appendix.

The pairing gap Δ and the renormalized chemical potential μ at $T < T_{ins}$ are obtained by solving simultaneously the non-linear gap equation and the equation on $\mu(T)$. The set looks particularly simple at $T = 0$ (here $\mu = \mu(T = 0)$, $\Delta = \Delta(T = 0)$):

$$\begin{aligned}
1 &= \frac{\lambda}{2} \int_0^\Lambda d\varepsilon \frac{1}{\sqrt{(\varepsilon - \mu)^2 + \Delta^2}}, \\
E_F &= \frac{1}{2} \int_0^\Lambda d\varepsilon \left(1 - \frac{\varepsilon - \mu}{\sqrt{(\varepsilon - \mu)^2 + \Delta^2}} \right).
\end{aligned} \tag{6}$$

Solving these equations we obtain at $T = 0$

$$\begin{aligned}
\mu + \sqrt{\mu^2 + \Delta^2} &= 2E_F \\
\sqrt{\mu^2 + \Delta^2} - \mu &= 2E_0
\end{aligned} \tag{7}$$

hence

$$\begin{aligned}
\mu &= E_F - E_0 \\
\Delta &= 2\sqrt{E_F E_0}
\end{aligned} \tag{8}$$

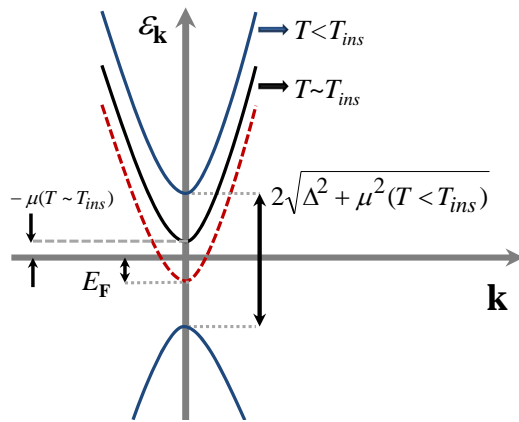


FIG. 4: The dispersion in the one-band model. Red dashed line – the bare dispersion (the one which the system would have at $T = 0$ in the absence of the pairing). Black line – the dispersion right above T_{ins} , blue line – the dispersion below T_{ins} . The plot is for the case when the chemical potential μ is already negative at $T = T_{ins}$. Observe that the minimal gap is $\sqrt{\Delta^2 + \mu^2}$ and the minimum of the dispersion is at $k = 0$ rather than at k_F .

These results were first obtained in Ref.¹³.

When $E_F \gg E_0$, the expressions for μ and Δ are the same as in BCS theory:

$$\begin{aligned}
\mu &\approx E_F, \\
\Delta &= 2(\lambda E_F)^{1/2} e^{-\frac{1}{\lambda}} = 1.76 T_{ins}.
\end{aligned} \tag{9}$$

In the opposite limit $E_F \ll E_0$,

$$\begin{aligned}
\mu &\approx -E_0 \\
\Delta &\sim T_{ins} \left(\frac{E_F}{E_0} \right)^{1/2} \log \frac{E_0}{E_F}.
\end{aligned} \tag{10}$$

Observe that while $\Delta = 2\sqrt{E_F E_0}$ stays the same in both limits, the ratio Δ/T_{ins} changes: $\Delta \sim T_{ins}$ at $E_F \gg E_0$ and $\Delta \ll T_{ins}$ at $E_F \ll E_0$. At $E_F = 0$, Δ , T_{ins} , and Δ/T_{ins} all vanish. The vanishing of Δ is easy to understand – a finite gap would reconstruct fermionic dispersion and open up a hole band with a finite density of carriers proportional to Δ , what is impossible at $E_F = 0$ because the density of fermions is zero. A negative μ implies that the Fermi momentum k_F (defined as position of the minimum of $E_k = \sqrt{(\varepsilon_k - \mu)^2 + \Delta^2}$) is zero. In fact, the Fermi momentum shifts downwards already in the normal state at a finite T because $\mu(T) < E_F$. It becomes zero at $T = T_{ins}$ at $E_0/E_F \approx 0.882$. The downward renormalization of k_F has been recently obtained in the study of superconductor-insulator transition.¹⁶

In Fig. 4 we plot the actual dispersion below and above T_{ins} along with the bare fermionic dispersion (the one which the system would have at $T = 0$ in the absence of the pairing). We emphasize that the gapping of excitations above T_{ins} (the black line in Fig. 4) is just the consequence of the temperature variation of the chemical potential and as such is not related to pairing.

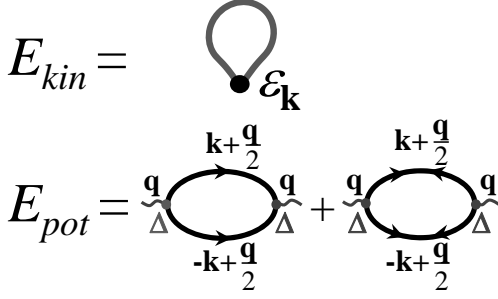


FIG. 5: Diagrammatic representation of the kinetic and potential energy of a one-band superconductor. The sum $E_{kin} + E_{pot}(q = 0)$ gives the condensation energy, and the prefactor for the q^2 term in $E_{pot}(q)$ determines the superfluid stiffness.

B. Superconducting T_c

The temperature T_{ins} appears in the ladder approximation as the transition temperature, but is actually only the crossover temperature as pair formation by itself does not break the gauge symmetry. To obtain the actual T_c , at which the gauge symmetry is broken (i.e., the phases of bound pairs order), one needs to treat the phase $\phi(r)$ as fluctuating variable and compute the energy cost of phase variation $\delta E = (1/2)\rho_s(T) \int dr |\nabla\phi|^2$ (see Refs. [38,39] for a generic description of fluctuations in superconductors). The prefactor $\rho_s(T)$ is the superfluid stiffness. In 2D, the superconducting transition temperature $T_c \sim \rho_s(T_c)$ (see, e.g., Refs. [40,41]). The interplay between T_c and T_{ins} depends on the ratio $\rho_s(T=0)/T_{ins}$. If this ratio is large, the superfluid stiffness rapidly increases below T_{ins} . In this situation, $T_c = T_{ins}$ minus a small correction, i.e., the phases of bound pairs order almost immediately after the pairs develop (phase fluctuations cost too much energy). If $\rho_s(T=0)/T_{ins}$ is small, $\rho_s(T)$ increases slowly below T_{ins} and T_c is of or-

der $\rho_s(T=0) \ll T_{ins}$.

The superfluid stiffness ρ_s has been evaluated before by looking at the diamagnetic tensor^{19,42,45,46}. We show below how one can extract the stiffness directly from the d -dependent condensation energy.

Within our model with local interaction U , δE is the $O(q^2)$ term in the ground state energy of an effective model described by the effective fermionic Hamiltonian with the anomalous term

$$\begin{aligned} \mathcal{H}_{anom} &= \int d^2r \Delta(r) c_{\uparrow}^{\dagger}(r) c_{\downarrow}^{\dagger}(r) + h.c \\ &= \sum_{k,q} \Delta(q) c_{\uparrow}^{\dagger}(k + q/2) c_{\downarrow}^{\dagger}(-k + q/2) + h.c \end{aligned} \quad (11)$$

with $\Delta(r) = \Delta e^{i\phi(r)} \approx \Delta e^{i(\nabla\phi)r}$ whose Fourier component $\Delta(q) = \Delta\delta(q - \nabla\phi)$.

The ground state energy is the sum of the kinetic and the potential energy. The kinetic energy depends on $|\Delta(r)|^2 = \Delta^2$ and is not sensitive to phase fluctuations (i.e., it does not have $(\nabla\phi)^2$ term) and is simply given by the convolution of the quasiparticle dispersion with a single fermionic Green's function (see Fig.5). At $T = 0$

$$\begin{aligned} E_{kin} &= 2N_0 \int \frac{d\varepsilon_k d\omega}{2\pi} \varepsilon_k G_s(k, \omega) = \\ &= -2N_0 \int \frac{d\varepsilon_k d\omega}{2\pi} \varepsilon_k \frac{i\omega + (\varepsilon_k - \mu)}{\omega^2 + (\varepsilon_k - \mu)^2 + \Delta^2} \end{aligned} \quad (12)$$

where G_s is the normal of the superconducting Green's function.

The potential energy, on the other hand, does depend on q . Within the model of Eq. (11) it is given by the sum of the convolutions of two normal and two anomalous Green's functions with Δ in the vertices^{18,38,42} (see Fig. 3). In the analytic form

$$E_{pot}(q) = -\Delta^2 \int \frac{d^2k d\omega}{(2\pi)^3} [G_s(k + q/2, \omega) G_s(-k + q/2, -\omega) + F_s(k + q/2, \omega) F_s(-k + q/2, -\omega)], \quad (13)$$

where F_s is the anomalous Green's function. Integrating over frequency in Eq.(13) we obtain at $T = 0$

$$\begin{aligned} E_{pot}(q) &= -\frac{\Delta^2}{|U|} + \frac{\Delta^2}{4} \int d^2k \frac{(\varepsilon_{k+q/2} - \varepsilon_{k-q/2})^2}{((\varepsilon_k - \mu)^2 + \Delta^2)^{3/2}} + \dots \\ &= -\frac{\Delta^2}{|U|} + q^2 \frac{\Delta^2}{8\pi} \int d\varepsilon_k \frac{\varepsilon_k}{((\varepsilon_k - \mu)^2 + \Delta^2)^{3/2}} + \dots \end{aligned} \quad (14)$$

where dots stand for the terms of higher orders in q^2 . The difference between $E_{pot}(q=0) + E_{kin}$ in a superconductor and the kinetic energy in the normal state gives

the condensation energy E_{cond} . To obtain E_{cond} we evaluate the frequency integrals in (12) and (14) and write the condensation energy as

$$\begin{aligned} E_{cond} &= -N_0 \times \\ &= \left[E_F^2 + \frac{\Delta^2}{2} \int_{-\mu}^{\Lambda} \frac{dx}{\sqrt{x^2 + \Delta^2}} \left(1 - \frac{2(x + \mu)}{x + \sqrt{x^2 + \Delta^2}} \right) \right] \end{aligned} \quad (15)$$

The integral over x is ultra-violet convergent and one can

safely replace the upper limit by infinity. We then obtain

$$E_{cond} = -N_0 \left[E_F^2 + \frac{\Delta^2}{4} - \frac{\mu}{2} \left(\mu + \sqrt{\mu^2 + \Delta^2} \right) \right] \quad (16)$$

Using $\mu = E_F - E_0$ and $\Delta^2 = 4E_F E_0$ (see Eq. (8)) we immediately obtain $\mu + \sqrt{\mu^2 + \Delta^2} = 2E_F$ and $\mu \left(\mu + \sqrt{\mu^2 + \Delta^2} \right) / 2 = E_F^2 - \Delta^2/4$. Substituting into (16) we obtain

$$E_{cond} = -N_0 \frac{\Delta^2}{2} = -N_0 E_0 E_F \quad (17)$$

no matter what the ratio E_F/E_0 is.

The prefactor for the q^2 term in Eq.(14) determines $\rho_s(T=0)$:

$$\rho_s(T=0) = N_0 \frac{\Delta^2}{8} \int d\varepsilon_k \frac{\left(\frac{d\varepsilon_k}{dk} \right)^2}{\left((\varepsilon_k - \mu)^2 + \Delta^2 \right)^{3/2}} \quad (18)$$

Using

$$\frac{\Delta^2}{\left((\varepsilon_k - \mu)^2 + \Delta^2 \right)^{3/2}} = -\frac{d}{d\varepsilon_k} \left(1 - \frac{\varepsilon_k - \mu}{\left((\varepsilon_k - \mu)^2 + \Delta^2 \right)^{1/2}} \right) \quad (19)$$

and integrating by parts Eq.(18) we obtain

$$\rho_s(T=0) = \frac{N_0}{8} \int d\varepsilon_k \times \left(1 - \frac{\varepsilon_k - \mu}{\left((\varepsilon_k - \mu)^2 + \Delta^2 \right)^{1/2}} \right) \left[\frac{d}{d\varepsilon_k} \left(\frac{d\varepsilon_k}{dk} \right) \right]^2 \quad (20)$$

The term in square brackets is simply a constant ($= 2/m$), and the remaining integral gives exactly the total energy density equal to $2E_F$. As a result,

$$\rho_s = \frac{E_F}{4\pi} \quad (21)$$

This result is exact for the parabolic dispersion $\frac{k^2}{2m}$, which we consider in this paper⁴³. The consideration based on diamagnetic tensor shows (Refs.^{19,42,45,46}) that it also holds, up to corrections of order $(E_0^2 + E_F^2)/\Lambda^2$, for arbitrary lattice dispersion.

At $E_F \gg E_0$, ρ_s is parametrically larger than $T_{ins} \sim (E_F E_0)^{1/2}$. As the consequence, phase fluctuations are costly and $T_c \approx T_{ins}$, i.e., fermionic pairs condense almost immediately after they develop. In the opposite limit $E_F \ll E_0$, $\rho_s(T=0) \ll T_{ins}$, and hence $T_c \sim \rho_s(T=0) \ll T_{ins}$. Using the criterium⁴⁰ $T_c = (\pi/2)\rho_s(T)$ and approximating $\rho_s(T)$ by $\rho_s(T=0)$, we obtain an estimate $T_c = E_F/8$. (A more accurate analysis⁴⁴ yields $T_c \sim E_F/\log(\log E_0/E_F)$.)

The superconducting transition temperature approaches zero as $O(E_F)$ when $E_F \rightarrow 0$, while $T_{ins} \sim E_0/\log \frac{E_0}{E_F}$ drops only logarithmically. The ratio T_c/T_{ins} scales as $\frac{E_F}{E_0} \log \frac{E_0}{E_F}$ and obviously vanishes when $E_F = 0$.

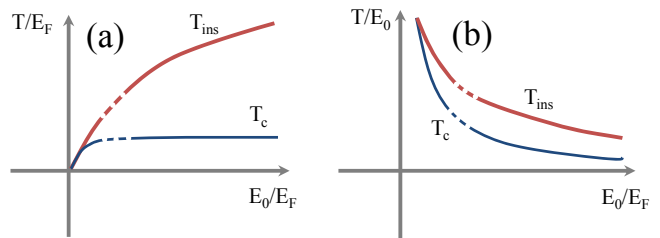


FIG. 6: The onset temperature T_{ins} for the bound state formation and the superconducting transition temperature T_c in the one-band model as functions of E_0/E_F . The temperatures are normalized to E_F (a) and E_0 (b). Dashed lines show T_c and T_{ins} in the intermediate regime $E_F/E_0 = O(1)$, where we didn't obtain the explicit formulas. Observe that T_{ins} scales as $E_0/\log E_0/E_F$ at large E_0/E_F . This T_{ins} increases when plotted in units of E_F and decreases when plotted in units of E_0 .

In the temperature region between T_{ins} and T_c the bound pairs develop but remain incoherent.

The splitting between T_{ins} and T_c once E_F gets smaller than T_{ins} (BCS-BEC crossover) and the corresponding preformed pairs behavior at $T_{ins} > T > T_c$ has been originally studied in 3D systems.^{14,15,20} The physics in 2D is similar, however in 2D the splitting occurs already at weak coupling, provided that E_F is small enough. Also, the distance between fermions in a bound pair (the coherence length ξ_0) scales at $\Delta \ll |\mu|$ as $\xi_0 \sim \left(\frac{1}{m|\mu|} \right)^{1/2} \sim 1/(mE_0)^{1/2}$. Like in 3D systems, this ξ_0 is much smaller than inter-fermion spacing $(V/N)^{1/2} \sim 1/(mE_F)^{1/2}$. On the other hand, $\xi - 0$ is much larger than the interatomic distance $a_0 \sim 1/(m\Lambda)^{1/2} \sim 1/q_{max}$, where $q_{max} = (2m\Lambda)^{1/2}$. (the ratio $\xi_0/a_0 \sim (\Lambda/E_0)^{1/2} \gg 1$). As a result, fermions in a bound pair are on average located much farther away from each other than interatomic spacing. Hence, the pairs cannot be viewed as nearest-neighbor "molecules" in the real space.

We summarize the results for the one-band model in Fig. 6, where we plot T_{ins} and T_c in units of E_F and E_0 , in both cases as functions of E_0/E_F .

Our results for both T_c and T_{ins} differ from Refs.^{8,30}. In these references T_c was found to remain finite at $E_F = 0$. The authors of^{8,30} solved BCS-like equations, hence their T_c is in fact the onset temperature for the pairing, T_{ins} . Still, we found that even this temperature vanishes at $E_F = 0$, once one includes into consideration temperature variation of the chemical potential.

C. The density of states at $T = 0$

In a conventional BCS superconductor with $E_F \gg T_c$, $\mu(T=0)$ is positive, and the density of states (DOS) at $T = 0$ is, for electron dispersion

$$\begin{aligned}
N(\omega) &= -\frac{1}{\pi} \text{Im} \int \frac{d^2k}{4\pi^2} G_s(k, \omega) = \int \frac{d^2k}{4\pi^2} (u_k^2 \delta(\omega - E_k) + v_k^2 \delta(\omega + E_k)) \\
&= \frac{N_0}{2} \left(\frac{2\omega}{\sqrt{\omega^2 - \Delta^2}} \theta(\omega - \Delta) - \frac{\omega - \sqrt{\omega^2 - \Delta^2}}{\sqrt{\omega^2 - \Delta^2}} \theta\left(\omega - \sqrt{\mu^2 + \Delta^2}\right) \right) \\
&+ \frac{N_0}{2} \left(\frac{2|\omega|}{\sqrt{\omega^2 - \Delta^2}} \theta(-\omega - \Delta) - \frac{|\omega| + \sqrt{\omega^2 - \Delta^2}}{\sqrt{\omega^2 - \Delta^2}} \theta\left(-\omega - \sqrt{\mu^2 + \Delta^2}\right) \right), \tag{22}
\end{aligned}$$

where $E_k = \sqrt{(\varepsilon_k - \mu)^2 + \Delta^2}$, $N_0 = m/(2\pi)$, $\theta(x) = 1$ for $x > 0$, $\mu = \mu(T = 0)$, and

$$\begin{aligned}
u_k^2 &= \frac{1}{2} \left(1 + \frac{\varepsilon_k - \mu}{\sqrt{(\varepsilon_k - \mu)^2 + \Delta^2}} \right), \\
v_k^2 &= \frac{1}{2} \left(1 - \frac{\varepsilon_k - \mu}{\sqrt{(\varepsilon_k - \mu)^2 + \Delta^2}} \right), \tag{23}
\end{aligned}$$

This $N(\omega)$ vanishes at $|\omega| < \Delta$, has a square-root singularity $1/\sqrt{|\omega - \Delta|}$ above the gap, and drops by a finite amount at $|\omega| = \sqrt{\mu^2 + \Delta^2} + 0$, when $|\omega|$ crosses the edge of the band. The DOS is nearly symmetric between positive and negative ω , at least for $\Delta < \omega \ll E_F$.

In our case, this behavior holds for the case $E_F \gg E_0$, but not for $E_F \ll E_0$. In the latter case, $\mu(T = 0)$ is negative ($\mu(T = 0) \approx -E_0$), and the DOS is given by

$$\begin{aligned}
N(\omega) &= -\frac{1}{\pi} \text{Im} \int \frac{d^2k}{4\pi^2} G_s(k, \omega) \\
&= \text{Im} \int \frac{d^2k}{4\pi^2} (u_k^2 \delta(\omega - E_k) + v_k^2 \delta(\omega + E_k)) \\
&= \frac{N_0}{2} \left(\frac{\omega + \sqrt{\omega^2 - \Delta^2}}{\sqrt{\omega^2 - \Delta^2}} \right) \theta\left(\omega - \sqrt{\mu^2 + \Delta^2}\right) \tag{24} \\
&+ \frac{N_0}{2} \left(\frac{|\omega| - \sqrt{\omega^2 - \Delta^2}}{\sqrt{\omega^2 - \Delta^2}} \right) \theta\left(-\omega - \sqrt{\mu^2 + \Delta^2}\right),
\end{aligned}$$

where $\mu = \mu(T = 0)$. This $N(\omega)$ vanishes at $|\omega| < \sqrt{\mu^2 + \Delta^2}$ and jumps to a finite value at $|\omega| = \sqrt{\mu^2 + \Delta^2} + 0$. Because $\mu \approx -E_0$, is much larger than $\Delta = 2(E_F E_0)^{1/2}$, the coherence factors u_k^2 and v_k^2 are quite different: $u_k^2 \approx 1$ for all momenta, while $v_k^2 \approx \frac{\Delta^2}{4(\varepsilon_k + |\mu|)}$ is small. As the result, $N(\omega)$ in (24) is highly anisotropic between positive and negative frequencies – it approaches N_0 at large positive frequencies and scales as $N_0 \Delta^2 / (4\omega^2)$ at large negative frequencies. We plot the DOS at zero temperature for $E_F \ll E_0$ in Fig. 7. Because only negative frequencies are probed in photoemission experiments, the features associated with the bound state development below T_{ins} are weak and disappear at $E_F \rightarrow 0$. This last feature has been also found in the recent study of superconductor-insulator transition.¹⁶

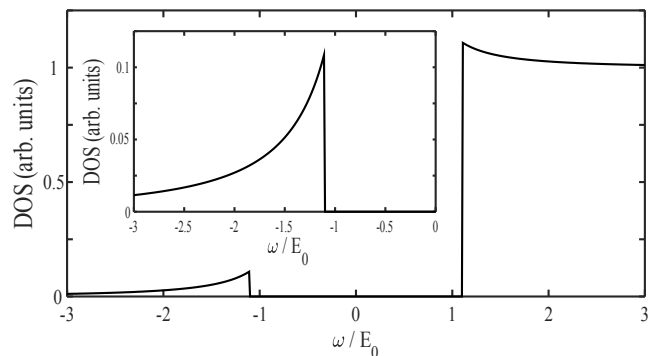


FIG. 7: The DOS in the single-band model at $T = 0$ for $E_F \ll E_0$. We set $E_F = 0.1E_0$, in which case $\mu = -9E_F$ and $\Delta = 2\sqrt{E_0 E_F} \approx 6.3E_F$. We added the fermionic damping $\gamma = 0.001E_F$. In the clean limit, the density of states vanishes at $|\omega| < \sqrt{\mu^2 + \Delta^2}$ and jumps to a finite value at $|\omega| = \sqrt{\mu^2 + \Delta^2} + 0$ (see Eq. (24)). Due to the difference between coherence factors, the DOS is strongly particle-hole anisotropic and has much larger value at positive frequencies, unobservable in photoemission experiments. At large $|\omega|$, the DOS tends to a finite value at positive ω and vanishes as $1/\omega^2$ at negative ω . To make the power-law suppression of the DOS at negative ω more visible, we plot the negative frequency region separately in the inset.

Note in passing that within our approximate treatment, based on the effective quadratic Hamiltonian, the DOS vanishes below $|\omega| = (\mu^2 + \Delta^2)^{1/2}$ already at $T < T_{ins}$. A more accurate treatment would require one to compute the imaginary part of the fermionic self-energy at a finite temperature and analyze the feedback on this self-energy from the development of the bound pairs. On general grounds, the density of states at $|\omega| < (\mu^2 + \Delta^2)^{1/2}$ should remain finite at temperatures between T_{ins} and T_c , as no symmetry is broken in this T range. Below T_c , however, the true gap develops at these frequencies and the DOS should be as in Fig. 7.

III. TWO-BAND MODEL WITH ONE HOLE AND ONE ELECTRON BAND

We now extend the analysis to two-band models. We consider two models – one with a hole and an electron

band, and one with two hole/two electron bands. In both cases we assume, to make presentation compact, that the dominant pairing interaction $U(q, \Omega)$ is the pair hopping between fermions on the two bands. The repulsive interaction of this type gives rise to s^{+-} pairing with the phase shift by π between Δ 's on the two bands.

In this section we consider the model with one band with hole-like dispersion $\varepsilon_k^h = E_{F,h} - \frac{k^2}{2m_h}$ and another with electron-like dispersion $\varepsilon_k^e = \frac{k^2}{2m_e} - E_{F,e}$. This model is relevant to FeSCs, at least, at a qualitative level. The Fermi energies $E_{F,h}$ and $E_{F,e}$ and the masses m_h and m_e are generally not equivalent. We keep $E_{F,h}$ and $E_{F,e}$ different, but set $m_h = m_e = m$ to simplify the formulas.

BCS analysis of the pairing in multi-band models with two electron bands and two or three hole bands, as in FeSCs, has been presented in series of recent publications^{8,30}. In particular, Ref.⁸ considered the case of two hole bands, only one of which crosses the Fermi level. A FS-constrained superconductivity in this last case emerges due to interaction between the hole band with $E_{F,h} > 0$ and the electron band(s). Ref.⁸ has demonstrated that the presence of the additional hole band increases T_c , despite that this band is full located below the Fermi level.

We analyze different physics – the crossover in the system behavior once the largest E_F becomes smaller than the two-particle bound state energy E_0 . This physics has not been analyzed before, to the best of our knowledge. We restrict to one hole and one electron band because the inclusion of additional bands affects the details of the analysis but does not qualitatively affect BCS-BEC crossover. Like in the previous Section, we set the upper energy cutoff at $\Lambda \gg E_{F,i}$ ($i = h, e$), approximate $U(q, \Omega)$ by a constant below the cutoff, and set the dimensionless coupling $\lambda = mU/(2\pi)$ to be small. We set $U > 0$, in which case superconducting order parameter has s^{+-} symmetry. As our goal is to analyze BCS-BEC crossover, we consider the particular case when $E_{F,e} = 0$, see Fig.3(b). The extension of the analysis to small but finite $E_{F,e}$ (positive or negative) is straightforward and does not bring qualitatively new physics.

The analysis of the bound state energy for two particles at $E_F \equiv 0$ does not differ from that in previous Section, and the result is that the scattering amplitude diverges at $T_0 = 1.13E_0$, where, like before, $E_0 = \Lambda e^{-2/\lambda}$. The bound state energy at $T = 0$ is $2E_0$.

The onset temperature for the pairing at a finite E_F is obtained by solving simultaneously the linearized equations for Δ_e and Δ_h and the equations for the chemical potentials $\mu_e(T)$ and $\mu_h(T)$, subject to $\mu_e(T) + \mu_h(T) = E_F$. The equation for the chemical potential follows for the conservation of the total number of fermions. The

set of equations is ($\mu_e = \mu_e(T_{ins}), \mu_h = \mu_h(T_{ins})$):

$$\begin{aligned}\Delta_e &= -\frac{\lambda}{2}\Delta_h \int_{-\mu_h}^{\Lambda} \frac{dx}{x} \tanh \frac{x}{2T_{ins}} \\ \Delta_h &= -\frac{\lambda}{2}\Delta_e \int_{-\mu_e}^{\Lambda} \frac{dx}{x} \tanh \frac{x}{2T_{ins}} \\ \mu_e &= T \log \frac{1 + e^{-\mu_h/T}}{1 + e^{\mu_e/T}} \\ \mu_e + \mu_h &= E_F.\end{aligned}\quad (25)$$

The first two equations reduce to

$$\frac{4}{\lambda^2} = \int_{-\mu_e}^{\Lambda} \frac{dx}{x} \tanh \frac{x}{2T_{ins}} \times \int_{-\mu_h}^{\Lambda} \frac{dx}{x} \tanh \frac{x}{2T_{ins}} \quad (26)$$

Below T_{ins} , Δ_e and Δ_h become non-zero and one has to consider non-linear gap equations and modify the equation for the chemical potential. At $T = 0$ the set of equations becomes [$\mu_h = \mu_h(T = 0), \mu_e = \mu_e(T = 0)$]:

$$\begin{aligned}\Delta_h &= -\frac{\lambda}{2}\Delta_e \log \frac{2\Lambda}{\sqrt{\mu_e^2 + \Delta_e^2} - \mu_e} \\ \Delta_e &= -\frac{\lambda}{2}\Delta_h \log \frac{2\Lambda}{\sqrt{\mu_h^2 + \Delta_h^2} - \mu_h} \\ \sqrt{\mu_h^2 + \Delta_h^2} + \mu_h - 2E_F &= \mu_e + \sqrt{\mu_e^2 + \Delta_e^2} \\ \mu_h + \mu_e &= E_F\end{aligned}\quad (27)$$

A. The case $E_F \gg E_0$

We assume and then verify that in this situation $T_{ins} \ll E_F$ and for all $T \leq T_{ins}$, $\mu_h \approx E_F$, while $\mu_e \sim T_{ins}$. Under these assumptions, the equations on the chemical potentials in (25) yield

$$\begin{aligned}\mu_e(T_{ins}) &= T_{ins} \log \frac{\sqrt{5} - 1}{2} = -0.48T_{ins}, \\ \mu_h(T_{ins}) &= E_F - \mu_e(T_{ins})\end{aligned}\quad (28)$$

Substituting these values of the chemical potentials into the first two equations in (25) we obtain after simple algebra

$$\begin{aligned}\Delta_e &= -\frac{\lambda}{2}\Delta_h \left[2 \log \frac{1.13\Lambda}{T_{ins}} - \frac{2}{\lambda} + \log \frac{E_F}{E_0} \right] \\ \Delta_h &= -\frac{\lambda}{2}\Delta_e \log \frac{1.13D\Lambda}{T_{ins}}\end{aligned}\quad (29)$$

where $D = 0.79$ ($\log D = -\int_0^{|\mu_e|/2T} dx \frac{\tanh x}{x}$). Combining the two equations and introducing $Z = \log \frac{1.13D\Lambda}{T_{ins}}$, we obtain at small λ ,

$$Z = \frac{2}{\lambda} - \frac{1}{3} \log \frac{E_F}{D^2 E_0} + O(\lambda). \quad (30)$$

Hence

$$T_{ins} = 1.13D^{1/3}E_F^{1/3}E_0^{2/3} = 1.04E_F^{1/3}E_0^{2/3} \quad (31)$$

This expression is valid when $\lambda \log E_F/E_0 \ll 1$. At even larger $E_F \leq \Lambda$, when $\lambda \log E_F/E_0 = O(1)$, T_{ins} is given by

$$T_{ins} \sim \Lambda \left(\frac{E_F}{\Lambda} \right)^{1/4} e^{-\frac{\sqrt{2}}{\lambda}} \quad (32)$$

The ratio of the gaps on electron and hole bands at $T = T_{ins} - 0$ is

$$\frac{\Delta_e}{\Delta_h} \approx - \left(1 + \frac{\lambda}{6} \log \frac{E_F}{E_0} \right) \quad (33)$$

We see that the gap on the electron band, which touches the Fermi level, is *larger* than the gap on the hole band, which crosses Fermi level. The ratio of Δ_e/Δ_h increases when E_F gets larger and approaches $\sqrt{2}$ when E_F becomes of order Λ .

At $T = 0$, solution of the set (27) at $E_F \gg E_0$ but $\lambda \log E_F/E_0 \ll 1$ shows that the ratio of Δ_e and Δ_h remains the same as in Eq. (33), i.e., up to subleading terms $\Delta_e(T = 0) = -\Delta_h(T = 0) = \Delta$. Solving for the chemical potentials we then find

$$\mu_e(T = 0) = -\frac{\Delta}{2\sqrt{2}}, \quad \mu_h(T = 0) = E_F - \mu_e(T = 0) \quad (34)$$

Substituting this into the first two equations in Eq. (27) and solving for Δ we obtain

$$\Delta = 2^{5/6}E_F^{1/3}E_0^{2/3} = 1.78E_F^{1/3}E_0^{2/3} \quad (35)$$

The minimum energy on the hole band is $E_h = \Delta$, at $k \approx k_F$. The minimum energy on the electron band is at $k = 0$, and $E_e = \sqrt{\mu_e^2(T = 0) + \Delta^2} = 3\Delta/2\sqrt{2} = 1.06\Delta$. For the ratio of the minimal energy to T_{ins} we then have, up to corrections of order $\lambda \log E_F/E_0$,

$$\frac{E_e}{T_{ins}} = 1.71, \quad \frac{E_h}{T_{ins}} = 1.81 \quad (36)$$

Note that both ratios are rather close to BCS values, although our consideration includes the renormalization of the chemical potential, neglected in BCS theory.

B. The case $E_F = E_0$

To establish the bridge to the case of small E_F/E_0 , consider the intermediate case when E_F is comparable to E_0 . To be specific, we just set $E_F = E_0$, although the analysis can be easily extended to arbitrary $E_F/E_0 \sim O(1)$. Because E_F is now the only relevant low-energy scale, we express $T_{ins} = aE_F, \mu_e(T_{ins}) =$

$bE_F, \mu_h(T_{ins}) = E_F(1-b)$. Substituting this into Eq.(25) and using the fact that

$$\frac{2}{\lambda} \int_0^\Lambda \frac{\tanh \frac{x}{2T_{ins}}}{x} = \frac{2}{\lambda} \log 1.13\Lambda/T_{ins} = 1 - \frac{2}{\lambda} \log \frac{a}{1.13}, \quad (37)$$

we obtain, to leading order in λ , the set of two equations on the prefactors a and b :

$$b = a \log \frac{1 + e^{\frac{b-1}{a}}}{1 + e^{\frac{b}{a}}}$$

$$2 \log \frac{a}{1.13} = \int_0^{\frac{b}{2a}} dy \frac{\tanh y}{y} + \int_0^{\frac{1-b}{2a}} dy \frac{\tanh y}{y} \quad (38)$$

Solving the set we obtain $T_{ins} = 1.351E_F, \mu_e(T_{ins}) = -0.349E_F$ and $\mu_h(T_{ins}) = 1.349E_F$. As expected, the chemical potential μ_e becomes negative at a finite temperature.

At $T = 0$ the renormalized chemical potentials $\mu_h(T = 0)$ and $\mu_e(T = 0)$ and the gaps Δ_h and Δ_e are also of order E_F . We express $\Delta_h = c_h E_F, \Delta_e = c_e E_F, \mu_e(T = 0) = \bar{b}E_F, \mu_h(T = 0) = E_F(1 - \bar{b})$. Substituting into Eq. (27) we obtain to leading order λ , $c_h = -c_e = c$, i.e., $\Delta_e \approx -\Delta_h$. [For non-equal masses m_h and m_e , $\Delta_h = \Delta(m_e/m_h)^{1/4}$, $\Delta_e = -\Delta(m_h/m_e)^{1/4}$]. The prefactors c and \bar{b} are the solutions of

$$\left(\sqrt{\bar{b}^2 + c^2} - \bar{b} \right) * \left(\sqrt{(1 - \bar{b})^2 + c^2} - (1 - \bar{b}) \right) = 4$$

$$\sqrt{(1 - \bar{b})^2 + c^2} - \sqrt{\bar{b}^2 + c^2} = 1 + 2\bar{b} \quad (39)$$

Solving this set we find $\bar{b} = -0.34$ and $c = 2.43$, i.e., $\mu_e(T = 0) = -0.34E_F, \mu_h(T = 0) = 1.34E_F$, and $\Delta_h \approx -\Delta_e = 2.43E_F$. We see that μ_e and μ_h change little between $T = T_{ins}$ and $T = 0$.

Because μ_e is negative, the minimal excitation energy for the electron band is (for $m_h = m_e$) $E_e = \sqrt{\mu_e^2 + \Delta^2} \approx 2.45E_F$. For the hole band, μ_h positive and the minimal energy is $E_h = \Delta$. We emphasize that the minimal energy E_e is larger than E_h , despite that the gaps Δ_e and Δ_h have equal magnitudes. The ratios of the minimal energy and T_{ins} are

$$\frac{E_e}{T_{ins}} = 1.82, \quad \frac{E_h}{T_{ins}} = 1.80 \quad (40)$$

Both are a bit larger than the BCS value of 1.76.

C. The case $E_F \ll E_0$

We assume and then verify that in this limit the onset temperature for the pairing T_{ins} and the gaps Δ_h and Δ_e become progressively larger than E_F , while μ_h and μ_e remain of order E_F . Assuming that $T_{ins} \gg E_F$ and

solving (25) for T_{ins} , we then immediately obtain

$$\begin{aligned} T_{ins} &= 1.13\Lambda e^{-\frac{2}{\lambda}} + \frac{E_F}{4} + O(\lambda) \approx 1.13E_0 \left(1 + 0.22 \frac{E_F}{E_0}\right) \\ &= T_0 \left(1 + 0.22 \frac{E_F}{E_0}\right) \end{aligned} \quad (41)$$

Note that this differs from BCS formula because the exponent contains $2/\lambda$ rather than $1/\lambda$. The reason is that only fermions with energies above E_F contribute to the logarithm. Solving the last two equations from Eq. (25), we obtain for the chemical potentials at $T = T_{ins}$

$$\mu_e(T_{ins}) \approx -\frac{E_F}{2}, \quad \mu_h(T_{ins}) \approx \frac{3E_F}{2} \quad (42)$$

Solving next for the gaps and the chemical potentials at $T = 0$ we obtain (for $m_h = m_e$) that the μ_e and μ_h move only little below T_{ins} , while $\Delta_h \approx -\Delta_e = \Delta$ is related to T_{ins} by the same formula as in BCS theory, i.e.,

$$\begin{aligned} \Delta &= 1.76T_{ins} \gg E_F \\ \mu_h &\approx \frac{3E_F}{2}, \quad \mu_e \approx -\frac{E_F}{2} \end{aligned} \quad (43)$$

The results for T_{ins} , Δ , and the chemical potential are all consistent with what we assumed a-priori, hence the computational procedure is self-consistent.

In Fig. 8 we plot the dispersions of fermions from hole and electron bands at $T > T_{ins}$ and $T \ll T_{ins}$ along with the bare dispersions (the one the system would have at $T = 0$ in the absence of the pairing). The figure is for the case $E_F < E_0$, the dispersion at $E_F > E_0$ is quite similar. Observe that the minimal energy of a fermion on the hole band (often associated with the "gap") is $\sqrt{\Delta_e^2 + \mu_e^2}$, while the minimal energy of a fermion on the electron band is just $|\Delta_h| \approx |\Delta_e|$, i.e., it is smaller.

Returning to Eq. (41), we notice that the temperature T_{ins} is only slightly higher than $T_0 = 1.13E_0$, at which the scattering amplitude for two particles in a vacuum diverges (to obtain T_0 one just has to set $E_F = 0$ in Eq.(41)). Like in the one-band case, this poses the question what is the actual T_c in this situation, because the development of the two-particle bound state does not generally imply the breaking of U(1) gauge (phase) symmetry. To understand what T_c is we need to compute superconducting stiffness. This is what we do next.

D. Superconducting T_c

We express U(1) order parameters Δ_e and Δ_h as $\Delta e^{-i\phi_e}$ and $\Delta e^{-i\phi_h}$ (we recall that, for equal masses $m_h = m_e$, the magnitudes of Δ_e and Δ_h are equal, up to small corrections). In the equilibrium $\phi_e - \phi_h = \pi$. To obtain the superfluid stiffness at $T = 0$ we need two ingredients^{45,46}: the gradient terms in the energy $(\nabla\phi_h)^2$, $(\nabla\phi_e)^2$, and $(\nabla\phi_h)(\nabla\phi_e)$, and the mixing term

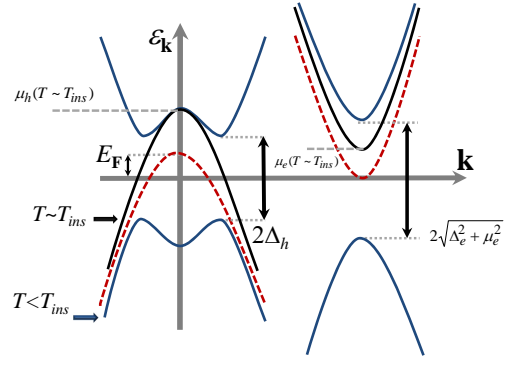


FIG. 8: Fermionic dispersions for the two-band model with one hole and one electron band in the limit $E_F \ll E_0$. Red dashed line – the bare dispersions (the one which the system would have at $T = 0$ in the absence of the pairing). Black lines – the dispersions right above T_{ins} , blue lines – the dispersion below T_{ins} . The chemical potential for the electron band is negative, and the minimal gap is $\sqrt{\Delta_e^2 + \mu_e^2}$. For the hole band, the chemical potential is positive and the dispersion $\pm\sqrt{\Delta_h^2 + (k^2/(2m) - \mu_h)^2}$ is non-monotonic, with the minimal energy Δ_h at $k_F = \sqrt{2m\mu_h}$. Note that this k_F is larger than the bare $k_{F,0} = \sqrt{2mE_F}$.

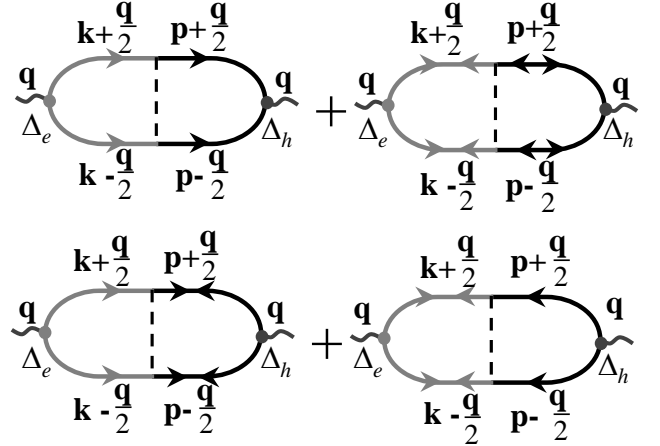


FIG. 9: Diagrammatic representation of the two-loop diagram for the potential energy $E_{pot}(q)$ in two-band models with a constant inter-band interaction U (the dashed line). Dark and light lines represent fermions from two different bands. The prefactor for q^2 term in $E_{pot}(q)$ determines the superfluid stiffness. For a constant (i.e., angle-independent) U , the q^2 term appear by expanding GG or FF terms either on the right side of on the left side of each diagram, but there is no cross-term from taking linear in q terms on the right and on the left.

$\Delta_e\Delta_h^* + \Delta_e^*\Delta_h \propto \cos(\phi_e - \phi_h)$. The last term is important when the stiffnesses on the hole and the electron bands substantially differ in magnitude because it generates the mass for phase fluctuations on the band with a smaller stiffness once the phase of the gap on the band with a larger stiffness gets ordered.

The prefactors for the gradient terms can be evaluated

in the same way as in the one-band model, by allowing the phases to vary as $e^{i(\nabla\phi)r}$, i.e., by taking the Fourier transform $\Delta(q) = \Delta\delta(q - \nabla\phi)$, and evaluating the prefactors for the q^2 terms in the potential energy (see Sec. II). The cross term $\nabla\phi_h\nabla\phi_e$ could potentially come from the two-loop diagram shown in Fig.9. There are no symmetry restrictions which would prevent the cross term to be present⁵¹, however, in our case the prefactor for $\nabla\phi_h\nabla\phi_e$ contains the integral $\int d\mathbf{k}d\mathbf{p}(\mathbf{q}\mathbf{k})(\mathbf{q}\mathbf{p})U(k-p)$ (\mathbf{k} is near an electron band, \mathbf{p} is near the hole band), which vanishes because we set $U(k-p)$ to be independent on the angle between \mathbf{k} and \mathbf{p} . The gradient part of the energy then comes solely from the bubbles made by fermions from the same band and is given by

$$\delta E_{gr} = \frac{1}{2}\rho_s^h(\nabla\phi_h)^2 + \frac{1}{2}\rho_s^e(\nabla\phi_e)^2 \quad (44)$$

The two-loop diagram, shown in Fig.9, however, gives rise to the mixed term $\Delta_e\Delta_h^* + \Delta_e^*\Delta_h$. To see this we evaluate this diagram at $q=0$. The sum of $G_s(k)G_s(-k)$ and $F_s(k)F_s(-k)$ terms in the right and in the left gives exactly $1/U$, hence

$$\delta E_{mix} = \frac{1}{U}(\Delta_e\Delta_h^* + \Delta_e^*\Delta_h) = \frac{\Delta^2}{U}\cos(\phi_e - \phi_h) \quad (45)$$

Without loss of generality we can assume that in equilibrium $\phi_e = 0$, $\phi_h = \pi$ (note that the overall sign in (44) is negative in equilibrium). Expanding in (45) to quadratic order in deviations of $\phi_{e,h}$ from the equilibrium values and combining (44) and (45), we obtain fluctuation part of the energy in the form

$$\delta E_{fl} = \frac{1}{2}\left[\rho_s^h(\nabla\tilde{\phi}_h)^2 + \rho_s^e(\nabla\tilde{\phi}_e)^2 + \frac{\Delta^2}{U}(\tilde{\phi}_e - \tilde{\phi}_h)^2\right], \quad (46)$$

where $\tilde{\phi}_{e,h}$ are deviations from equilibrium values. This δE_{fl} can be treated as an effective Hamiltonian for fluctuations of $\tilde{\phi}$ in the sense that $\langle\tilde{\phi}^2\rangle \propto \int d\tilde{\phi}e^{-\delta E_{fl}/T}$. This effective Hamiltonian can be also obtained by starting with fermionic Hamiltonian with 4-fermion interaction in the Cooper channel and using Hubbard-Stratonovich transformation to re-express the partition function as the integral over bosonic variables $\Delta_{e,h}(r) = |\Delta|e^{i\phi_{e,h}(r)}$ (see Refs.^{21,45-48}).

Transforming into the momentum space and evaluating $\langle|\tilde{\phi}_{e,h}(k)|^2\rangle$, we obtain

$$\begin{aligned} \langle|\tilde{\phi}_e(k)|^2\rangle &= \frac{T\left(k^2\rho_s^h + \frac{\Delta^2}{U}\right)}{k^4\rho_s^e\rho_s^h + \frac{\Delta^2}{U}k^2(\rho_s^e + \rho_s^h)} \\ \langle|\tilde{\phi}_h(k)|^2\rangle &= \frac{T\left(k^2\rho_s^e + \frac{\Delta^2}{U}\right)}{k^4\rho_s^e\rho_s^h + \frac{\Delta^2}{U}k^2(\rho_s^e + \rho_s^h)} \end{aligned} \quad (47)$$

If the mixing term was absent (i.e., if there was no Δ^2/U term in (47)), we would have $\langle|\tilde{\phi}_e(k)|^2\rangle = T/(\rho_s^e k^2)$ and $\langle|\tilde{\phi}_h(k)|^2\rangle = T/(\rho_s^h k^2)$, i.e., phase fluctuations of Δ_e and

Δ_h would be decoupled and the actual T_c , below which the system displays full coherence, would be determined by the smaller of the two stiffnesses. The presence of the mixed term changes the situation because now the ordering of one $\tilde{\phi}$ produces the mass term for fluctuations of the other phase variable. To estimate T_c we need to look at the small momentum asymptotic of Eq.(47) where

$$\langle|\tilde{\phi}_e(k)|^2\rangle = \langle|\tilde{\phi}_h(k)|^2\rangle = \frac{T}{(\rho_s^h + \rho_s^e)k^2}. \quad (48)$$

Hence T_c is determined by the combined stiffness $\rho_{comb} = \rho_s^e + \rho_s^h$. When $\rho_{comb} \gg T_{ins}$, phase fluctuations are costly and T_c almost coincides with T_{ins} . When $\rho_{comb} \ll T_{ins}$, we again use the approximate criterium $T_c \approx (\pi/2)\rho_{comb}(T) = 1.57\rho_{comb}(0)$.

We now proceed with the calculations of ρ_s^e and ρ_s^h . The q -dependent part of the energy for each band is again given by the sum of the convolutions of normal and anomalous Green's functions with the total momentum q , with Δ in the vertices, i.e., by the integrals of $\Delta^2(G_s(k+q/2)G_s(-k+q/2) + F_s(k+q/2)F_s(-k+q/2))$ (see Eq. (13)). Each stiffness at $T=0$ is then given by Eq. (18) with $\mu = \mu_e$ or μ_h , i.e.,

$$\begin{aligned} \rho_s^e(T=0) &= \frac{\Delta_e^2}{8\pi} \int_0^\Lambda d\varepsilon \frac{\varepsilon}{((\varepsilon - \mu_e)^2 + \Delta_e^2)^{3/2}} \\ \rho_s^h(T=0) &= \frac{\Delta_h^2}{8\pi} \int_0^\Lambda d\varepsilon \frac{\varepsilon}{((\varepsilon - \mu_h)^2 + \Delta_h^2)^{3/2}}. \end{aligned} \quad (49)$$

Using the same manipulations as in Sec. II B, one can relate ρ_s^h and ρ_s^e to the total number of fermions in the hole and the electron band, N_h and N_e . The two are given by

$$\begin{aligned} N_e &= N_0 \int_0^\Lambda d\varepsilon \left(1 - \frac{\varepsilon - \mu_e}{\sqrt{(\varepsilon - \mu_e)^2 + \Delta_e^2}}\right) \\ N_h &= N_0 \int_0^\Lambda d\varepsilon \left(1 + \frac{\varepsilon - \mu_h}{\sqrt{(\varepsilon - \mu_h)^2 + \Delta_h^2}}\right), \end{aligned} \quad (50)$$

and the relations are

$$\frac{N_e}{N_0} = 8\pi\rho_s^e, \quad \frac{N_h}{N_0} = 2\Lambda - 8\pi\rho_s^h \quad (51)$$

The conservation of the total number of particles implies that $N_h + N_e = 2N_0(\Lambda - E_F)$, hence

$$\rho_s^h - \rho_s^e = \frac{E_F}{4\pi} \quad (52)$$

This condition, however, only specifies the difference between ρ_s^h and ρ_s^e , the combined stiffness ρ_{comb} is not fixed and depends on the ratio E_F/E_0 , as we see below.

At $E_F \gg E_0$ we obtained from Eq.(49), using $\Delta \ll E_F$ and $\mu_e(T=0) = -\frac{\Delta}{2\sqrt{2}}$, $\mu_h(T=0) = E_F - \mu_e(T=0) \approx E_F$:

$$\begin{aligned} \rho_s^h(T=0) &\approx \frac{E_F}{4\pi}, \\ \rho_s^e(T=0) &\approx 0.71\frac{\Delta_h}{8\pi} = 0.05T_{ins} \ll \rho_s^h(T=0), \end{aligned} \quad (53)$$

where, we remind, $T_{ins} \sim \Delta \sim (E_F E_0^2)^{1/3} \ll E_F$. Adding the two stiffnesses, we find $\rho_{comb}(T=0) \approx E_F/(4\pi) \gg T_{ins}$. The inequality $\rho_{comb} \gg T_{ins}$ implies that phase fluctuations are costly and hence $T_c \approx T_{ins}$.

Note in passing that at $E_F \gg E_0$, $T/(\rho_{comb} k^2)$ behavior of the the Fourier transform of the correlation function for phase fluctuations holds in the full momentum range where the gradient expansion is applicable. Indeed, gradient expansion holds when k is smaller than inverse superconducting coherence length $\xi^{-1} = \Delta/v_F$. Comparing the mixed term Δ^2/U with even the larger $k^2 \rho_s^h \sim k^2 E_F$, we find that at $k \sim \xi^{-1}$, $k^2 \rho_s^h \sim m \Delta^2$ is already parametrically smaller than $\Delta^2/U \sim (m \Delta^2)/\lambda$. Hence Eq. (47) is valid for all $k < \xi^{-1}$.

At $E_F = E_0$ we obtain from Eq.(49), using the results for $\Delta_{e,h}$ and $\mu_{e,h}$ from Sec. IIIB,

$$\rho_s^h(T=0) = 2.05 \frac{E_F}{4\pi}, \quad \rho_s^e(T=0) = 1.05 \frac{E_F}{4\pi} \quad (54)$$

Observe that $\rho_s^h(T=0) - \rho_s^e(T=0) = E_F/(4\pi)$, as it should be, according to (52). Combining the two we obtain $\rho_{comb} = 3.1 E_F/(4\pi)$. Using $T_c \approx 1.57 \rho_{comb}$ we obtain $T_c \approx 0.39 E_F$. The onset temperature for the pair formation is $T_{ins} = 1.35 E_F \approx 3.49 T_c$. We see that now T_{ins} is substantially larger than T_c , hence already at $E_F = E_0$ the system should display preformed pair behavior in a wide range of temperatures.

Finally, at $E_F \ll E_0$ the chemical potentials $\mu_{e,h} \sim E_F$ are parametrically smaller than Δ . In this situation we obtain from Eq.(49)

$$\rho_s^h \approx \rho_s^e \approx \frac{\Delta^2}{8\pi} \int_0^\infty d\varepsilon \frac{\varepsilon}{(\varepsilon^2 + \Delta^2)^{3/2}} = \frac{\Delta}{8\pi} = 0.07 T_{ins}. \quad (55)$$

Hence

$$\rho_{comb} = 0.14 T_{ins}, \quad T_c \approx 0.22 T_{ins} \quad (56)$$

This holds even when $E_F = 0$, i.e., when the electron band is empty. The stiffnesses ρ_s^h and ρ_s^e are equal in this limit, as required by (52) but each remains non-zero and of order T_{ins} . As the consequence, T_c remains finite and also of order T_{ins} . Still, because numerically $T_c \ll T_{ins}$, there exists a sizable temperature range of preformed pair behavior.

Because now T_{ins} almost coincides with the temperature T_0 of bound state formation for two particles in a vacuum, the change of system behavior between $E_F \gg E_0$ and $E_F \ll E_0$ can be interpreted as BEC phenomenon. We emphasize, however, that the ratio of $\frac{T_{ins}}{T_c}$ remains finite at $E_F \rightarrow 0$, in distinction to ordinary BCS-BEC crossover, where this ratio tends to infinity when E_F vanishes.¹³

The still existence of a finite T_c at vanishing E_F is in variance with the situation in the one-band model and, as we will see in the next Section, also with the two-band model with two electron/two hole bands. There, T_c vanishes when $E_F = 0$ on both bands. The difference can

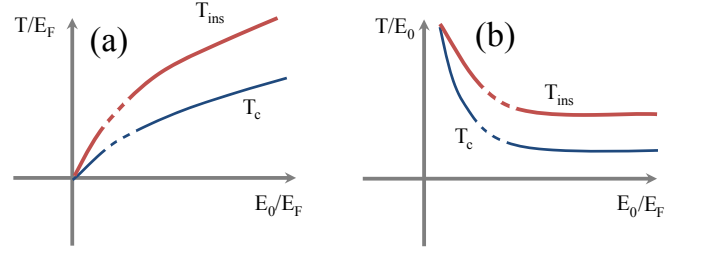


FIG. 10: The onset temperature T_{ins} for the bound state formation and the superconducting transition temperature T_c in the two-band model with one hole and one electron Fermi surface, as functions of E_0/E_F . The temperatures are in units of E_F (a) and E_0 (b). Observe that both T_{ins} and T_c scale as E_0 at large E_0/E_F .

be easily understood because in the other two models there are no carriers at $E_F = 0$ to form superconducting condensate, hence the gap must vanish at $E_F = 0$, otherwise there would appear an image band at negative energies with a finite density of carriers in it. In the model with a hole and an electron band there is charge reservoir in the hole band, and the charge density can be re-distributed into the image bands even at $E_F = 0$. The image of the electron band appears at negative energies $E = -\sqrt{\Delta_e^2 + (\varepsilon_k^e - \mu_e)^2}$. The states in this new band are filled by electrons, and their total density is given by $N_0 \int d\varepsilon_k \left(1 - \frac{\varepsilon_k^e - \mu_e}{\sqrt{\Delta_e^2 + (\varepsilon_k^e - \mu_e)^2}}\right) \sim \Delta \sim T_{ins}$. The electrons from the filled states in this image band can form superconducting condensate, and, because all energy scales are of order T_{ins} , superconducting T_c is also a fraction of T_{ins} .

Note also that at $E_F \ll E_0$, the Fourier transform of the correlation function for phase fluctuations is given by $T/(\rho_{comb} k^2) = T/(2\rho_s^h k^2)$ at the lowest k , but crosses over to a similar but not identical expression at larger k , which are still smaller than ξ^{-1} . The reasoning is that $k^2 \rho_s^h \approx k^2 \rho_s^e$ becomes comparable to the mixing term Δ^2/U at $k_{typ} \sim \xi^{-1} (E_F/\lambda E_0)^{1/2}$, which, at small enough E_F , is smaller than ξ^{-1} . In between k_{typ} and ξ^{-1} , the correlation function scales as $T/(\rho_s^h k^2)$, i.e., the functional form is the same as at the smallest k but the prefactor differs by 2.

Our results for T_c and T_{ins} in the model with one hole and one electron pocket are summarized in Fig. 10. Like in Fig. 6, we plot T_c and T_{ins} in units of either E_0 or E_F , both times as functions of E_0/E_F . We re-iterate that the key result for this model is that both T_{ins} and T_c scale as E_0 at large E_0/E_F .

E. The density of states at $T = 0$

The DOS in the model with one hole and one electron band is different from that in the one-band model because now fermionic excitations in the normal state exist

at both positive and negative frequencies. In the main parts of the two panels in Fig.11 we show the behavior of the DOS at $T = 0$ separately for hole and electron bands, $E_0 = E_F$ and $E_0 \gg E_F$, respectively. The behavior of the DOS on the electron band is very similar to that in the one-band model (see Eq. (24) and Fig.6). Namely, the DOS vanishes at $|\omega| < \sqrt{\Delta_e^2 + \mu_e^2}$ and jumps to a finite value at $|\omega| = \sqrt{\Delta_e^2 + \mu_e^2} + 0$. The DOS is highly anisotropic between negative and positive frequencies due to anisotropy of coherence factors. It is much larger at positive frequencies, where it tends to a finite value at large ω . At negative frequencies, the discontinuity is weaker (and rapidly suppressed by a fermionic damping), and the DOS falls off as $1/\omega^2$ for larger negative frequencies. On the hole band, the DOS vanishes at $|\omega| < |\Delta_h|$ and has a BCS-like square-root singularity at $|\omega| = |\Delta_h| + 0$, symmetric between negative and positive frequencies. At larger $|\omega|$, the DOS on the hole band has a discontinuity at $|\omega| = \sqrt{\Delta_h^2 + \mu_h^2} - 0$, when $|\omega|$ crosses the edge of the band and the corresponding momentum $k = 0$ (see Eq. (22); for hole dispersion positive and negative frequencies in (22) have to be interchanged). In the normal state this would be van-Hove discontinuity at the top of the hole band. In a superconductor, the discontinuity holds for both positive and negative ω , but the coherence factor is much larger for a positive ω . At higher frequencies, the DOS on the hole band tends to a finite value at negative frequencies and scales as $1/\omega^2$ at positive frequencies.

In the insets of Fig.11 we show the total (combined) DOS for $E_0 = E_F$ and $E_0 \gg E_F$. Observe that DOS tends to a finite value at both positive and negative frequencies.

IV. TWO-BAND MODEL WITH TWO ELECTRON BANDS

In this section we analyze the model with two bands of equal type. The results are identical for the model with two hole bands and for the one with two electron bands. For definiteness we consider the model with two electron bands as in Fig.3(c). We consider the same electronic configuration at $T = 0$ as for one hole/one electron band model. Namely, we set the chemical potential to touch the bottom of one of the bands and cross the other band, i.e. the Fermi energy to zero in one band (band 2) and finite in the other (band 1). At the end of this Section we consider how the onset temperature for the pairing evolves when we move the chemical potential such that both bands cross the Fermi level. Like in the previous section, we restrict with inter-band (pair-hopping) pairing interaction.

The behavior of T_{ins} , Δ , μ , and ρ_s in the model with two electron bands (and in a more general model with intra-band pairing interaction) has been discussed analytically in Refs.⁵² for the case when $E_F \gg E_0$. The set of equations for T_{ins} , Δ , and μ has been solved numer-

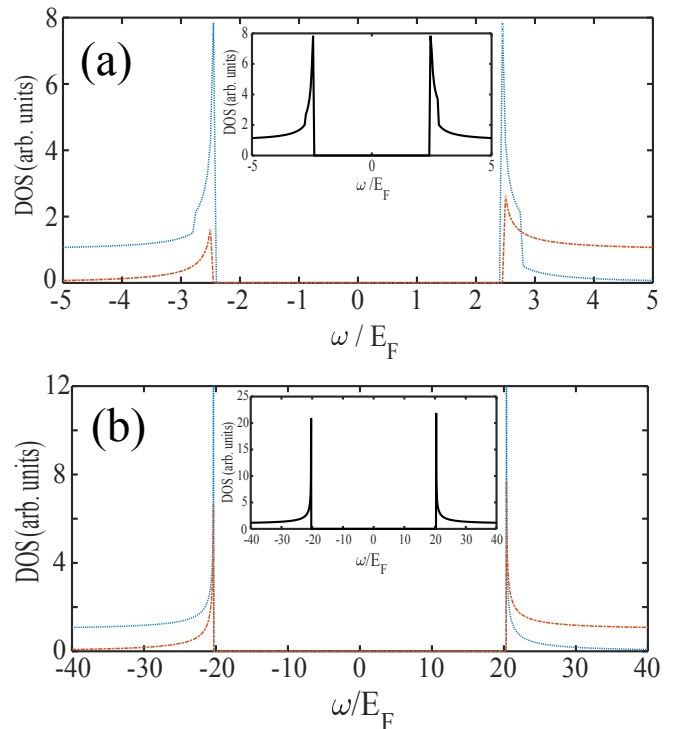


FIG. 11: The DOS at $T = 0$ for the model with one hole and one electron pocket. Panel (a) – $E_0 = E_F$, panel (b) – $E_0 = 10E_B$. For $E_0 = E_F$, $\mu_e = -0.34E_F$, $\mu_h = 1.34E_F$, and $\Delta_h \approx -\Delta_e = 2.43E_F$. For $E_F = 0.1E_0$, $\mu_h \approx \frac{3E_F}{2}$, $\mu_e \approx -\frac{E_F}{2}$, and $\Delta_e \approx -\Delta_h \approx 20.3E_F$. To cut the singularities and make other features of DOS visible, we added fermionic damping $\gamma = 0.001E_F$. Main figures – the DOS separately for the hole band (dashed blue) and the electron band (dashed red). For the hole band, the DOS has a square-root singularity at $|\omega| = |\Delta_h| + 0$, symmetric between negative and positive frequencies, and van-Hove discontinuity at $|\omega| = \sqrt{\Delta_h^2 + \mu_h^2} + 0$ (see Eq. (22); for hole dispersion positive and negative frequencies in (22) have to be interchanged). The latter is stronger for positive frequencies, due to anisotropy of coherence factors. For $E_F = 0.1E_0$, the singularity and the discontinuity are almost undistinguishable. For the electron band, the DOS jumps to finite value at $|\omega| = \sqrt{\Delta_e^2 + \mu_e^2} + 0$ and is highly anisotropic between negative and positive frequencies, again due to anisotropy of the coherence factors (see Eq. (24)). For $E_F = 0.1E_0$, $\Delta \gg \mu_e$, and the DOS right after the jumps are large, of order Δ/μ_e . Insets – the total DOS. Observe that at large frequencies the total DOS tends to a finite value for both positive and negative ω .

ically for arbitrary E_F/E_0 (Refs.^{20,26}). When the comparison is possible, our results agree with these works, but we also present new analytical results for T_{ins} , Δ , μ , and the superfluid stiffness for the cases when $E_F \sim E_0$ and $E_F < E_0$. The pairing at $E_F \gg E_0$ has been considered recently in Refs.^{22,31}. Our results agree with these earlier works modulo that they computed T_{ins} without including into consideration the temperature dependence of the chemical potential in the band 2, while we argue

that this renormalization is $O(1)$ effect.

The analysis of the bound state energy for two particles at $E_F \equiv 0$ does not differ from that in previous Sections, and the result is that the scattering amplitude diverges at $T_0 = 1.13E_0$, where, like before, $E_0 = \Lambda e^{-2/\lambda}$. The bound state energy at $T = 0$ is $2E_0$.

The onset temperature for the pairing at a finite E_F is obtained by solving simultaneously the linearized equations for Δ_1 and Δ_2 and the equations for the chemical potentials $\mu_1(T)$ and $\mu_2(T)$, subject, in this case, to $\mu_1(T) - \mu_2(T) = E_F$. The set of equations is ($\mu_1 = \mu_1(T_{ins}), \mu_2 = \mu_2(T_{ins})$):

$$\begin{aligned}\Delta_1 &= -\frac{\lambda}{2}\Delta_2 \int_{-\mu_2}^{\Lambda} \frac{dx}{x} \tanh \frac{x}{2T_{ins}} \\ \Delta_2 &= -\frac{\lambda}{2}\Delta_1 \int_{-\mu_1}^{\Lambda} \frac{dx}{x} \tanh \frac{x}{2T_{ins}} \\ E_F &= T \log \left[\left(1 + e^{\mu_1/T}\right) \times \left(1 + e^{\mu_2/T}\right) \right] \\ \mu_1 - \mu_2 &= E_F\end{aligned}\quad (57)$$

The first two equations reduce to

$$\frac{4}{\lambda^2} = \int_{-\mu_1}^{\Lambda} \frac{dx}{x} \tanh \frac{x}{2T_{ins}} \times \int_{-\mu_2}^{\Lambda} \frac{dx}{x} \tanh \frac{x}{2T_{ins}} \quad (58)$$

Below T_{ins} , Δ_1 and Δ_2 become non-zero and one has to consider non-linear gap equations and modify the equation for the chemical potential. At $T = 0$ we have [$\mu_1 = \mu_1(T = 0), \mu_2 = \mu_2(T = 0)$]:

$$\begin{aligned}\Delta_1 &= -\frac{\lambda}{2}\Delta_2 \log \frac{2\Lambda}{\sqrt{\mu_2^2 + \Delta_2^2} - \mu_2} \\ \Delta_2 &= -\frac{\lambda}{2}\Delta_1 \log \frac{2\Lambda}{\sqrt{\mu_1^2 + \Delta_1^2} - \mu_1} \\ 2E_F &= \sqrt{\mu_1^2 + \Delta_1^2} + \sqrt{\mu_2^2 + \Delta_2^2} + \mu_1 + \mu_2 \\ \mu_1 - \mu_2 &= E_F\end{aligned}\quad (59)$$

A. The case $E_F \gg E_0$

Like we did in the previous Section, we assume and then verify that $T_{ins} \ll E_F$ and that at $T = T_{ins}$, $\mu_1 \approx E_F$, while $\mu_2 \sim T_{ins}$. Under these assumptions, the equations on the chemical potentials in (57) yield ($\mu_{1,2} \equiv \mu_{1,2}(T_{ins})$)

$$\mu_2 = T \log \left(\frac{1}{1 + e^{\mu_2 T}} \right), \quad \mu_1 = E_F + \mu_2 \quad (60)$$

Solving for μ_2 we obtain

$$\mu_2 = T_{ins} \log \frac{\sqrt{5} - 1}{2} = -0.48T_{ins}, \quad \mu_1 = E_F - 0.48T_{ins} \quad (61)$$

This is the same result as Eq. (28). Substituting these results into the first two equations in (25) we obtain after simple algebra

$$\begin{aligned}\Delta_2 &= -\frac{\lambda}{2}\Delta_1 \left[2 \log \frac{1.13\Lambda}{T_{ins}} - \frac{2}{\lambda} + \log \frac{E_F}{E_0} \right] \\ \Delta_1 &= -\frac{\lambda}{2}\Delta_2 \log \frac{1.13D\Lambda}{T_{ins}}\end{aligned}\quad (62)$$

where $D = 0.79$. Solving the set we obtain

$$T_{ins} = 1.13D^{1/3}E_F^{1/3}E_0^{2/3} = 1.04E_F^{1/3}E_0^{2/3} \quad (63)$$

in full similarity with Eq. (31) for the model with a hole and an electron pocket. Like in that case, Eq. (63) is valid when $\lambda \log E_F/E_0 \ll 1$. At even larger $E_F \leq \Lambda$, when $\lambda \log E_F/E_0 = O(1)$, T_{ins} is given by

$$T_{ins} \sim \Lambda \left(\frac{E_F}{\Lambda} \right)^{1/4} e^{-\frac{\sqrt{2}}{\lambda}} \quad (64)$$

The ratio of the gaps on electron and hole bands at $T = T_{ins} - 0$ is

$$\frac{\Delta_2}{\Delta_1} \approx - \left(1 + \frac{\lambda}{6} \log \frac{E_F}{E_0} \right) \quad (65)$$

We see that the gap on the band which touches the Fermi level is *larger* than the gap on the band, which crosses Fermi level, in full agreement with the case of one hole and one electron band. This result holds even when the full band 2 is located above the Fermi level. The ratio of Δ_2/Δ_1 increases when E_F gets larger and approaches $\sqrt{2}$ when E_F becomes of order Λ .

At $T = 0$, the solution of the set (59) at $E_F \gg E_0$ but $\lambda \log E_F/E_0 \ll 1$ shows that the ratio of Δ_1 and Δ_2 remains the same as in Eq. (65), i.e., up to subleading terms $\Delta_1(T = 0) = -\Delta_2(T = 0) = \Delta$. Solving for the chemical potentials we then find ($\mu_{1,2} \equiv \mu_{1,2}(T = 0)$)

$$\mu_2 = -\frac{\Delta}{2\sqrt{2}}, \quad \mu_1 = E_F + \mu_2 \quad (66)$$

Substituting this into the first two equations in Eq. (59) and solving for Δ we obtain

$$\Delta = 2^{5/6}E_F^{1/3}E_0^{2/3} = 1.78E_F^{1/3}E_0^{2/3} \quad (67)$$

B. The case $E_F = E_0$

Like we did in the previous section, we express $T_{ins} = aE_F, \mu_1(T_{ins}) = bE_F, \mu_2(T_{ins}) = E_F(b-1)$. Substituting these relations into Eq.(57) and using the fact that

$$\frac{2}{\lambda} \int_0^{\Lambda} \frac{\tanh \frac{x}{2T_{ins}}}{x} = \frac{2}{\lambda} \log 1.13\Lambda/T_{ins} = 1 - \frac{2}{\lambda} \log \frac{a}{1.13}, \quad (68)$$

we obtain, to leading order in λ , the set of two equations on a and b :

$$1 = a \log \left[\left(1 + e^{\frac{b-1}{a}} \right) \times \left(1 + e^{\frac{b}{a}} \right) \right]$$

$$2 \log \frac{a}{1.13} = \int_0^{\frac{b}{2a}} dy \frac{\tanh y}{y} + \int_0^{\frac{b-1}{2a}} dy \frac{\tanh y}{y} \quad (69)$$

Solving the set we obtain $T_{ins} = 0.924E_F$, $\mu_1(T_{ins}) = 0.115E_F$, and $\mu_2(T_{ins}) = -0.885E_F$. As expected, the chemical potential μ_2 becomes negative at a finite temperature.

At $T = 0$ we express $\Delta = \bar{c}E_F$, $\mu_1(T = 0) = \bar{b}E_F$, $\mu_2(T = 0) = (\bar{b} - 1)E_F$. Substituting into Eq. (59) we obtain the set of two equations

$$\left(\sqrt{\bar{b}^2 + \bar{c}^2} - \bar{b} \right) \times \left(\sqrt{(\bar{b} - 1)^2 + \bar{c}^2} + (1 - \bar{b}) \right) = 4$$

$$\sqrt{(\bar{b} - 1)^2 + \bar{c}^2} + \sqrt{\bar{b}^2 + \bar{c}^2} = 3 - 2\bar{b} \quad (70)$$

Solving this set we find $\bar{c} = 1.38$ and $\bar{b} = -0.05$, i.e., $\mu_1(T = 0) = -0.05E_F$, $\mu_2(T = 0) = -1.05E_F$, and $\Delta_1 \approx -\Delta_2 = 1.38E_F$. We see that μ_1 changes from a slightly positive to a slightly negative value between $T = T_{ins}$ and $T = 0$.

C. The case $E_F \ll E_0$

We assume and then verify that at small E_F both μ_1 and μ_2 become negative at $T = T_{ins}$, and each exceeds E_F by magnitude. Solving Eq. (57) under these assumptions we obtain

$$\mu_1(T_{ins}) = -\frac{T_{ins}}{2} \log \frac{T_{ins}}{E_F} + \frac{E_F}{2},$$

$$\mu_2(T_{ins}) = -\frac{T_{ins}}{2} \log \frac{T_{ins}}{E_F} - \frac{E_F}{2} \quad (71)$$

Substituting these chemical potential into the equation for T_{ins} an solving it, we obtain

$$T_{ins} = \frac{4.52E_0}{\log \frac{E_0}{E_F}} \quad (72)$$

This T_{ins} has the same functional form as T_{ins} for the one-band model in the same limit $E_F \ll E_0$. This T_{ins} scales as E_0 , up to a logarithmic factor, but still vanishes at $E_F = 0$ due to logarithmic suppression.

Plugging T_{ins} from (72) back into (71) we obtain $\mu_1 \approx \mu_2 \approx -2.51E_0$, what justifies the assumption we made.

Solving next for the gaps and chemical potentials at $T = 0$, we obtain (for $m_h = m_e$) that $\mu_1 \approx \mu_2 \approx -E_0$, while $\Delta_1 \approx -\Delta_2 = \Delta$, where

$$\Delta = \sqrt{2} \sqrt{E_F E_0} \ll T_{ins} \quad (73)$$

The expression for the gap also agrees, up to an overall factor, with that in the one-band model.

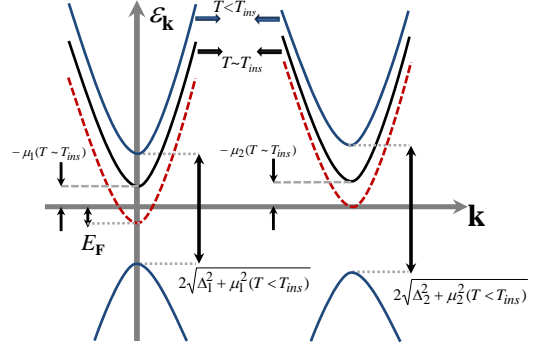


FIG. 12: Fermionic dispersions for the two-band model with two electron bands in the limit $E_F \ll E_0$. Red dashed line – the bare dispersions (the one which the system would have at $T = 0$ in the absence of the pairing). Black lines – the dispersions right above T_{ins} , blue lines – the dispersion below T_{ins} . The chemical potentials for both bands are now negative at $T \geq T_{ins}$ and in the BEC state below T_{ins} , and the minimal gaps on each band is $\sqrt{\Delta^2 + \mu^2}$. The minimum of dispersion on both bands is at $k = 0$. This is very similar to the behavior of the one-band model (see Fig. 4).

In Fig. 12 we plot the actual dispersion of the two electron bands below T_{ins} for the case $E_F \ll E_0$, along with the bare dispersion. We see that the system behavior is very similar to that in the one-band model (see Fig. 4 for comparison).

To understand what T_c is we again need to compute superconducting stiffness.

D. Superconducting T_c

We follow the same logics as in the previous section, i.e., introduce coordinate-dependent phases of the gaps on the two electron bands $\phi_1(r)$ and $\phi_2(r)$, compute the prefactors for the gradient term in the ground state energy $E_{gr} = (1/2)\rho_{s,1}(\nabla\phi_1)^2 + (1/2)\rho_{s,2}(\nabla\phi_2)^2$ and the mixing term $(\Delta^2/U) \cos(\phi_1 - \phi_2)$. Performing the same calculations as in the previous Section, we find that T_c is determined by the combined stiffness $\rho_{comb} = \rho_{s,1} + \rho_{s,2}$.

The stiffnesses $\rho_{s,1}$ and $\rho_{s,2}$ are expressed via $\Delta_{1,2}$ and $\mu_{1,2}$ by the same formulas as we obtained in the previous two Sections:

$$\rho_{s,1}(T = 0) = \frac{\Delta_1^2}{8\pi} \int_0^\Lambda d\varepsilon \frac{\varepsilon}{((\varepsilon - \mu_1)^2 + \Delta_1^2)^{3/2}}$$

$$\rho_{s,2}(T = 0) = \frac{\Delta_2^2}{8\pi} \int_0^\Lambda d\varepsilon \frac{\varepsilon}{((\varepsilon - \mu_2)^2 + \Delta_2^2)^{3/2}}. \quad (74)$$

The two stiffnesses are again related to the number of fermions in each band via $N_1 = 8\pi N_0 \rho_{s,1}$, $N_2 = 8\pi N_0 \rho_{s,2}$. Accordingly,

$$\rho_{comb} = \rho_{s,1} + \rho_{s,2} = \frac{E_F}{4\pi} \quad (75)$$

At $E_F \gg E_0$, $\rho_{comb} \gg T_{ins}$, hence $T_c \approx T_{ins}$. The two individual stiffnesses are

$$\begin{aligned} \rho_{e,2}(T=0) &\approx 0.03\Delta = 0.05T_{ins} \ll E_F \\ \rho_{s,1}(T=0) &\approx \frac{E_F}{4\pi}. \end{aligned} \quad (76)$$

This result is essentially identical to the one for the model with a hole and an electron pocket in the same limit.

For $E_F = E_0$, we obtain from Eq.(74), using the results for $\Delta_{e,h}$ and $\mu_{e,h}$ from Sec. IV B,

$$\begin{aligned} \rho_{s,1}(T=0) &= 0.053E_F, \\ \rho_{s,2}(T=0) &= 0.027E_F, \\ \rho_{comb}(T=0) &= 0.08E_F \equiv \frac{E_F}{4\pi} \end{aligned} \quad (77)$$

Treating $1/(4\pi)$ as a small parameter and using the same estimate of the actual T_c as before we obtain $T_c \approx 0.125E_F$. The onset temperature for the pair formation is $T_{ins} = 0.924E_F \approx 7.4T_c$. Hence the system again displays preformed pair behavior in a wide range of temperatures. .

Finally, for $E_F \ll E_0$, both μ_1 and μ_2 tend to $-E_0$, the gap behaves as $\Delta_1^2 = \Delta_2^2 = 2E_FE_0$. Substituting into Eq.(74) we obtain

$$\rho_{s,1} \approx \rho_{s,2} = \frac{E_F}{8\pi}, \quad \rho_{comb} = \frac{E_F}{4\pi} \quad (78)$$

Hence $T_c \sim E_F$ and is parametrically smaller than $T_{ins} \sim E_0/\log(E_0/E_F)$, i.e., there is a parametrically wide range of preformed pair behavior. This behavior is quite similar to the one in the canonical BEC regime, but we caution that T_{ins} is still smaller by a large logarithm than the temperature $T_0 \sim E_0$ at which a bound state of two fermions emerges in a vacuum.

We summarize the results for the model with two electron bands in Fig. 13. The behavior of T_c and T_{ins} in this model is quite similar to that in the model with one electron bands. A similar behavior also holds in the models with one or two hole bands.

E. The density of states at $T=0$

The DOS at $T=0$ in the model with two electron bands is quite similar to that in the one-band model. Namely, the DOS is highly anisotropic and is much larger at positive frequencies than at negative frequencies. For $E_F \ll E_0$, the chemical potentials are large and negative on both bands, and the DOS on each band is zero at $|\omega| < \sqrt{\mu^2 + \Delta^2}$, displays a discontinuity at $|\omega| = \sqrt{\mu^2 + \Delta^2} + 0$, and at large negative frequencies scales as $1/\omega^2$ (see Eq. (22)). We show the DOS for this model for $E_F = E_0$ and $E_F = 0.1E_0$ in Fig. 14

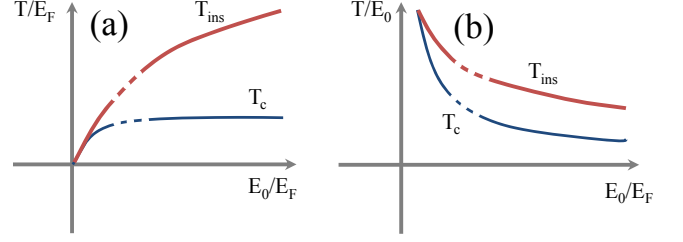


FIG. 13: The onset temperature T_{ins} for the bound state formation and the superconducting transition temperature T_c in the two-band model with two electron bands, as functions of E_0/E_F . The temperatures are normalized to E_F (a) and to E_0 (b). Like in the case of one-band model, T_{ins} scales as $E_0/\log E_0/E_F$ at large E_0/E_F , while T_c scales as E_F .

F. Evolution of T_{ins} and T_c with the filling of the second band and comparison with the experiments on Nb-doped SrTiO₃

Like we said in the Introduction, superconductivity in the model with two electron bands is realized experimentally in Nb-doped SrTiO₃ and, possibly, in heterostructures of LaAlO₃ and SrTiO₃ (see Ref.³¹ and references therein). The Fermi energy in the band 1 is finite already at zero doping, and E_F is likely larger than E_0 , in which case $T_c \approx T_{ins}$. The band 2 is above the chemical potential at zero doping, but the chemical potential at $T=0$ moves up with doping and enters the band 2 once it exceeds the critical value.

The experiments have found that superconducting T_c rapidly increases when the chemical potential enters the band 2. This has been detected in Nb-doped SrTiO₃ (Ref. [32]) and in LaAlO₃/SrTiO₃ heterostructures (Ref. [33]).

To verify whether this effect can be explained within our theory, we extend our approach to the case when E_F is finite in both bands. To make notations more convenient, in this subsection we use μ instead of E_F (see Fig. 3.) We count μ from the bottom of the band 1, hence the bare chemical potential μ_0 (the one at $T=0$ and $\Delta=0$) coincides with E_F in this band. We assume that at $T=0$ the chemical potential in the band 2 is $\mu_0 - \mu^*$. At zero doping $\mu^* > \mu_0$. At a finite doping, μ_0 increases and crosses μ^* at some finite doping. Once μ_0 gets larger than μ^* , the chemical potential enters the band 2. We set $\mu_0 = \mu^* + \epsilon$, assume that $|\epsilon| \ll \mu_0$, and obtain the correction to T_c to first order in ϵ .

At a finite temperature, the chemical potentials in the two bands satisfy $\mu_1 = \mu_0 - \epsilon + \mu_2$ and the condition that the total number of particles is conserved reads

$$\mu_0 + \epsilon = T \log \left[(1 + e^{\mu_1/T}) \times (1 + e^{\mu_2/T}) \right] \quad (79)$$

The onset temperature for the pairing, $T_{ins} \approx T_c$ is obtained by solving the set of linearized gap equations for

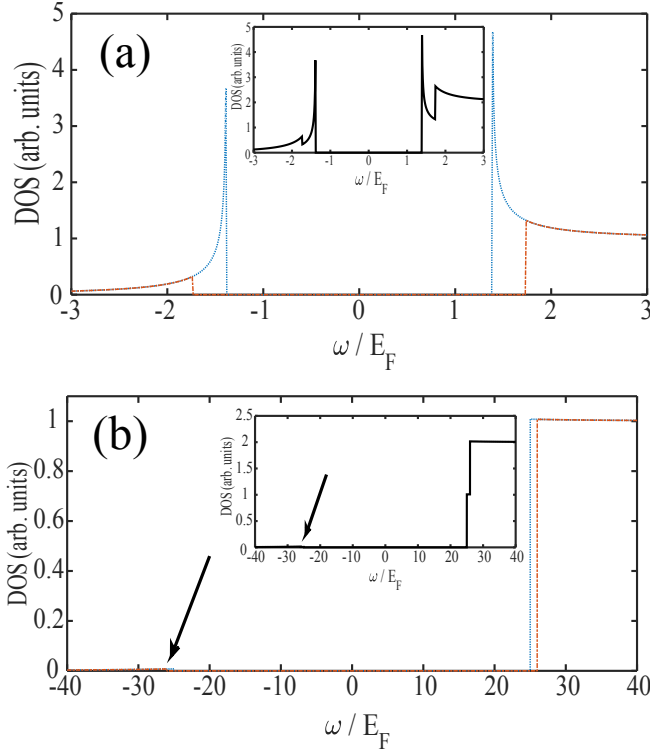


FIG. 14: The DOS at $T = 0$ for the model with two electron bands. Panel (a) – $E_0 = E_F$, panel (b) – $E_0 = 10E_B$. For $E_0 = E_F$, $\mu_1 = -0.05E_F$, $\mu_2 = -1.05E_F$, and $\Delta_1 \approx -\Delta_e = 1.38E_F$. For $E_0 = 10E_B$, $\mu_1 \approx -24.6E_F$, $\mu_2 \approx -25.6E_F$, and $\Delta_1 \approx \Delta_2 = 4.47E_F$. We introduced the damping $\gamma = 0.001E_F$ to make all features of the DOS visible. Main figures – the DOS for each band (dashed red and blue lines). Insets – the total DOS. In the clean limit, the DOS has a discontinuity at $|\omega| = \sqrt{\Delta_i^2 + \mu_i^2} + 0$ ($i = 1, 2$), like in the one-band model. At $E_0 = E_F$, DOS on band 1 is large immediately after the jump because μ_1 is very small. The DOS for each band is anisotropic between negative and positive frequencies due to anisotropy of the coherence factors. At large frequencies, the DOS tends to a finite value for positive ω and scales as $1/\omega^2$ for negative ω . The arrow in panel (b) indicates the position of the would be discontinuity at a negative frequency.

Δ_1 and Δ_2 . The set has the same form as in Eq. (57):

$$\begin{aligned}\Delta_1 &= -\frac{\lambda}{2}\Delta_2 \int_{-\mu_2}^{\Lambda} \frac{dx}{x} \tanh \frac{x}{2T_{ins}} \\ \Delta_2 &= -\frac{\lambda}{2}\Delta_1 \int_{-\mu_1}^{\Lambda} \frac{dx}{x} \tanh \frac{x}{2T_{ins}}\end{aligned}\quad (80)$$

We assume that $\mu_0 \gg E_0$. The analysis in Sec. (IV A) for $\mu^* = \mu_0$ shows that $T_{ins} \ll \mu_0$, and, by continuity, we assume that this remains true for $\mu^* \approx \mu_0$. One easily make sure that for such T_{ins} , $\mu_1(T_{ins}) \approx \mu_0 \gg T_{ins}$. Eq. (79) then reduces to

$$\mu_2 - 2\epsilon = -T_{ins} \log(1 + e^{\mu_2/T_{ins}}) \quad (81)$$

Solving this equation we find

$$\mu_2 = -T_{ins} \log \frac{2}{\sqrt{5}-1} + \frac{4\epsilon}{\sqrt{5}(\sqrt{5}-1)} \quad (82)$$

Solving then the linearized gap equation to first order in ϵ we obtain after a simple algebra

$$T_{ins}(\epsilon) = T_{ins}(0) + \frac{2\epsilon}{3\sqrt{5}(\sqrt{5}-1)} \quad (83)$$

where $T_{ins}(0) = 1.04E_0^{2/3}\mu_0^{1/3}$. Re-expressing this result back in terms of μ_0 and μ^* we obtain

$$T_{ins}(\epsilon) = T_{ins}(0) \left[1 + 0.23 \frac{\mu_0 - \mu^*}{\mu_0} \left(\frac{\mu_0}{E_0} \right)^{2/3} \right] \quad (84)$$

We see that T_{ins} and hence $T_c \approx T_{ins}$ increases once μ_0 gets larger than μ^* , and the slope is controlled by the large factor $(\mu_0/E_0)^{2/3}$, i.e., the relative increase is parametrically large. By the same reason, T_c rapidly decreases when μ_0 is smaller than μ . That T_c increases once μ_0 gets larger than μ^* has been earlier found numerically in BCS calculations in Ref. [22,31]. Our results are consistent with this work, however we emphasize that (i) our analytical result, Eq. (84) shows that the slope of T_c vs $\mu_0 - \mu^*$ is parametrically enhanced at $\mu_0 \gg E_0$ and (ii) "pure" BCS calculation neglects the thermal evolution of the chemical potential, while in our analysis this renormalization is included and plays an important role.

A rapid increase of T_c once the band 2 gets populated in consistent with the data^{32,33}. At the same time, our T_c is continuous as a function of μ , i.e., we didn't find a jump in T_c at a critical doping, as suggested in e.g.,³⁴.

V. THE GMB FORMALISM

A somewhat different approach to superconductivity in a situation when E_F is much smaller than the upper energy cutoff for the pairing interaction was put forward by GMB in Ref. [35]. They considered weak coupling 3D case and argued that, from the physics point of view, T_c has to be expressed in terms of observable quantum-mechanical scattering amplitude taken in the limit of zero momentum (the scattering length, a) rather than in terms of unobservable interaction potential U . The relation between U with a is obtained by solving Schrödinger equation for one particle in a field U of another particle. Diagrammatically, this amounts to summing up ladder series vertex correction diagrams in the particle-particle channel for two particles in a vacuum, i.e., for zero chemical potential. To first order in U , $a = mU/(4\pi)$ and the dimensionless coupling constant $\lambda = m|U|/(2\pi^2)$ (in 3D) equals to $(2|a|k_F)/\pi$. However, beyond leading order, λ and $(2|a|k_F)/\pi$ are not equivalent.

GMB have demonstrated that, with logarithmic accuracy, the equation for T_c in terms of a is obtained by summing up the same ladder series as in the BCS theory,

however, two modifications have to be made simultaneously: (i) U has to be replaced by $4\pi a/m$, and (ii) in each ladder cross-section one has to subtract from the product of the two Green's functions $G_{k,\omega}G_{-k,-\omega}$ the same GG term taken at zero chemical potential. As the result of these modifications, the kernel in the gap equation is cut at energies of order E_F , and E_F appears as a prefactor in the formula for T_c , once the exponent contains $\pi/(2|a|k_F)$ instead of $1/\lambda$. GMB went further than logarithmic approximation and obtained the exact weak coupling formula $T_c = 0.277E_F e^{-\pi/(2|a|k_F)}$ by adding the leading renormalizations from the particle-hole channel. We discuss these renormalizations in the Appendix. The GMB approach does not include phase fluctuations and hence the instability temperature obtained in this approach is actually the onset temperature for the pairing, T_{ins} .

Below we discuss the extension of GMB approach to 2D case and show how our T_{ins} can be re-expressed in terms of the physical scattering amplitude. We obtain T_{ins} in the form $T_{ins} = E_F * f(a)$, where a is the scattering amplitude (dimensionless in 2D). These formulas are useful if a is known from some other experiment. We show that in the proper limits $T_{ins} \gg E_F$ because $f(a)$ is large.

We consider one-band model and two-band model with

one hole and one electron pocket. The analysis of the model with two electron pockets is equivalent to that of the one-band model. We show that GMB approach is applicable for arbitrary ratio of E_F/E_0 , including the regime where T_{ins} is close to the temperature T_0 , at which the scattering amplitude diverges.

To set the stage, we first briefly review GMB approach in 3D and then consider 2D cases.

A. Original GMB consideration, weak coupling $D = 3$ case

To keep presentation short, we only restrict with the ladder series and neglect contributions from the particle-hole channel, i.e., will not try to reproduce the exact prefactor for T_{ins} .

GMB argued that to properly express T_{ins} in terms of observable variables, one has to consider simultaneously the ladder series for the pairing vertex Φ in terms of bare Φ_0 and ladder series for the vertex function $\Gamma = 4\pi|a|/m$ for two particles in a vacuum in terms of the interaction U . The ladder series are easily obtained diagrammatically and reduce to

$$\begin{aligned}\Phi &= \Phi_0 \left[1 + \Pi_{pp}(E_F)|U| + (\Pi_{pp}(E_F)U)^2 + \dots \right] = \frac{\Phi_0}{1 - |U|\Pi_{pp}(E_F)} \\ \Gamma &= |U| \left[1 + \Pi_{pp}(0)|U| + (\Pi_{pp}(0)U)^2 + \dots \right] = \frac{|U|}{1 - |U|\Pi_{pp}(0)},\end{aligned}\quad (85)$$

where

$$\Pi_{pp}(\mu) = T \sum_{\omega_m} \int d^3k/(2\pi^3) G(k, \omega) G(-k, -\omega) = T \sum_{\omega_m} \int d^3k/(2\pi^3) (\omega_m^2 + (\varepsilon_k - \mu)^2)^{-1}.\quad (86)$$

Expressing $|U|$ in terms of Γ as $|U| = \Gamma/(1 + \Gamma\Pi_{pp}(0))$ and substituting into the expression for Φ we obtain

$$\Phi = \frac{\Phi_0^*}{1 - \Gamma(\Pi_{pp}(E_F) - \Pi_{pp}(0))}\quad (87)$$

where $\Phi_0^* = \Phi_0(1 + \Gamma\Pi_{pp}(0)) \sim \Phi_0$. Eq. (87) can be viewed as the sum of ladder series for Φ with $|U|$ replaced by $\Gamma = 4\pi|a|/m$ and the term with zero chemical potential subtracted from $\int GG$.

With these modifications, the equation for the instability temperature in terms of $|a|$ becomes:

$$1 = \frac{2|a|k_F}{\pi} \int_0^\Lambda d\varepsilon \left(\frac{\varepsilon}{E_F} \right)^{1/2} \left[\frac{\tanh \frac{\varepsilon - E_F}{2T_c}}{\varepsilon - E_F} - \frac{\tanh \frac{\varepsilon}{2T_c}}{\varepsilon} \right]\quad (88)$$

We remind that we consider the case $E_F \ll \Lambda$. One can easily check that the integral over ε now converges at $\varepsilon \sim E_F$, so the upper limit of integration doesn't matter any longer. The evaluation of the integral yields, at $|a|k_F \ll 1$,

$$T_c = 0.61E_F e^{-\frac{\pi}{2|a|k_F}}\quad (89)$$

This equation re-expresses T_{ins} in 3D in terms of the fully renormalized s-wave scattering length. The renormalizations from the particle-hole channel further change the prefactor to 0.277 (Ref.³⁵).

One can easily check that Eq. (89) coincides with the conventional BCS result for T_{ins} in 3D. Indeed, from the first equation in (85) we obtain T_{ins} in 3D directly in terms of U :

$$T_{ins} = \tilde{\Lambda} e^{-\frac{1}{\tilde{\lambda}}}\quad (90)$$

where $\tilde{\lambda} = m|U|k_F/(2\pi^2)$ (dimensionless coupling constant in 3D) and $\tilde{\Lambda} = 0.61E_F e^{\sqrt{\frac{\Lambda}{E_F}}}$. Using the weak-coupling relation between ak_F and $\tilde{\lambda}$:

$$\frac{2|a|k_F}{\pi} \approx \tilde{\lambda} \left(1 + \tilde{\lambda} \sqrt{\frac{\Lambda}{E_F}} \right) \quad (91)$$

one can easily verify that Eqs. (89) and (90) are equivalent, as they indeed should be.

We emphasize that, although Eqs. (89) and (90) are identical, the physics behind GMB approach in 3D is the separation of scales: fermions with energies below E_F are the only ones which contribute to superconductivity, while fermions with energies above E_F renormalize the interaction between low-energy fermions into the quantum-mechanical scattering amplitude.

B. Extension of GMB formalism to 2D

We now extend this approach to 2D case. We consider separately one-band and two-band models.

1. One-band model

We first consider the case $E_F > E_0$, when bound pairs do not develop prior to superconductivity and the scattering amplitude is small at weak coupling, and then extend the analysis to the case $E_F < E_0$.

In the 2D case the scattering amplitude, which we label a_2 , is dimensionless. To first order in $U < 0$ we still have $a_2 = mU/(4\pi)$. Keeping a_2 as a small parameter and performing GMB computation of T_{ins} in 2D, we obtain

$$T_{ins} = 1.13E_F e^{-\frac{1}{|a_2|}} \quad (92)$$

This equation is the 2D analog of Eq. (89). It expresses T_{ins} in terms of the 2D scattering amplitude, which is an observable variable.

Eq. (92) is the same as Eq. (4) for T_{ins} in terms of U , as we now demonstrate. Summing up ladder series of renormalizations which convert U into $ma_2/(4\pi)$, we obtain

$$\frac{1}{a_2} = \log \frac{1.13\Lambda}{T} - \frac{2}{\lambda} \quad (93)$$

where, we remind, $\lambda = m|U|/(2\pi)$. At $E_F > E_0$, $T_{ins} \sim (E_F E_0)^{1/2} \gg E_0$, hence at a_2 is negative at $T \sim T_{ins}$, like the interaction U . Substituting $1/|a_2| = -1/a_2$ from Eq.(93) into Eq.(92) we obtain

$$T_{ins} = 1.13(\Lambda E_F)^{1/2} e^{-\frac{1}{\lambda}} \quad (94)$$

This coincides with Eq. (4).

In the opposite limit $E_F \ll E_0$, the temperature T_{ins} is larger than E_F , hence the temperature dependence

of the chemical potential μ must be included into the GMB-type analysis. Performing the same calculation as before and treating a_2 as some temperature-dependent parameter, not necessary a small one, we obtain, using $\mu = -T \log T/E_F$:

$$\log \log \frac{T_{ins}}{E_F} = \frac{1}{a_2} \quad (95)$$

or

$$T_{ins} = E_F e^{e^{1/a_2}} \quad (96)$$

This formula again expresses T_{ins} in terms of the scattering amplitude a , with E_F as the overall factor.

Eq. (96) looks simple, but one should keep in mind that the scattering amplitude a_2 by itself depends on temperature. In view of this, T_{ins} is actually the solution of the transcendental equation $T = E_F \exp(\exp(1/a_2(T)))$, in which $a_2(T)$ should be treated as input function, extracted from independent measurements.

We now demonstrate that, although T_{ins} in Eq.(96) contains $E_F \ll E_0$ as the overall factor, this T_{ins} coincides with that in Eq.(5), once a_2 is re-expressed back in terms of λ . To see this we substitute $1/a_2$ from Eq.(93) into Eq.(95) and obtain

$$\log \frac{T_{ins}}{E_F} = e^{-\frac{2}{\lambda}} e^{\log \frac{1.13\Lambda}{T_{ins}}} = \frac{E_0}{T_{ins}} \quad (97)$$

or

$$T_{ins} = \frac{E_0}{\log \frac{E_0}{E_F}} \quad (98)$$

This is the same expression as Eq.(5) as it indeed should be.

Note that a_2 is actually positive at $T = T_{ins}$ because T_{ins} is smaller than $T_0 = 1.13E_0$ at which a bound state forms in a vacuum. Taken at a face value, this would reply that the interaction becomes repulsive. However, one can easily verify that $a_2(T_{ins})$ changes sign exactly when $\mu(T_{ins})$ crosses zero. As a result, $\int(GG(\mu) - GG(0))$ becomes negative simultaneously with the sign change of a and the product $a_2 * \int(GG(\mu) - GG(0))$ in the denominator of (87) remains positive.

The case when $T_{ins} \approx T_0$ actually requires more sophisticated treatment because the scattering amplitude is large at $T = T_{ins}$ and the corrections to the ladder diagrams, which we neglected, may become relevant. We will not pursue this case nor discuss the mathematical details how to properly extend the ladder series for the scattering amplitude in Eq.(93) to the case when a in Eq.(93) changes sign. We just consider the agreement between Eqs. (96) and (5) is the evidence that Eq. (93) can be used even when a_2 is not small.

C. Two-band model

We now extend GMB analysis to the two band model with a hole and an electron bands.

The inter-band scattering amplitude a_{he} is again obtained by summing up ladder diagrams for the vertex function for the two particles in a vacuum. Inter-band scattering is reproduced in odd orders in the interaction. We set $m_h = m_e$ to simplify calculations, sum up odd terms in the ladder series, and obtain

$$a_{he} = \frac{\lambda}{2} \frac{1}{1 - \frac{\lambda^2}{4} \Pi^2} \quad (99)$$

where $\Pi = \log 1.13\Lambda/T$ is the particle-particle polarization operator at $\mu = 0$. We remind that $\lambda = m|U|/(2\pi)$ in 2D.

Expressing λ in terms of a_{he} as

$$\lambda = \frac{4a_{he}}{1 + \sqrt{1 + 4a_{he}^2 \Pi^2}} \quad (100)$$

and substituting this back into the set of linearized equations for Δ_1 and Δ_e , Eqs. (25), we obtain after a simple algebra the equation for T_{ins} as a function of a_{he} :

$$2 + 2\sqrt{1 + 4a_{he}^2 \Pi^2} = 4a_{he}^2 (\Pi_e \Pi_h - \Pi^2) \quad (101)$$

where

$$\begin{aligned} \Pi_e &= \int_{-\mu_e}^{\Lambda} d\varepsilon \frac{\tanh \frac{\varepsilon}{2T}}{\varepsilon} \\ \Pi_h &= \int_{-\mu_h}^{\Lambda} d\varepsilon \frac{\tanh \frac{\varepsilon}{2T}}{\varepsilon} \end{aligned} \quad (102)$$

The r.h.s. of Eq.(101) can be re-written as

$$(\Pi_e \Pi_h - \Pi^2) = \tilde{\Pi}_e \tilde{\Pi}_h + \Pi (\tilde{\Pi}_e \tilde{\Pi}_h) \quad (103)$$

and

$$\begin{aligned} \tilde{\Pi}_e &= \Pi_e - \Pi = \int_0^{\mu_e} d\varepsilon \frac{\tanh \frac{\varepsilon}{2T}}{\varepsilon} \\ \tilde{\Pi}_h &= \Pi_h - \Pi = \int_0^{\mu_h} d\varepsilon \frac{\tanh \frac{\varepsilon}{2T}}{\varepsilon} \end{aligned} \quad (104)$$

Each $\tilde{\Pi}$ is $\int(GG(\mu) - GG(0))$, i.e., it is the difference between the particle-particle polarization operator at a finite chemical potential $\mu_{e,h}$ and the one at $\mu = 0$. The chemical potentials $\mu_{e,h}$ are at most of order E_F , hence the integrals in Eq.(104) come from energies below E_F , like in the original GMB analysis.

At small E_0/E_F , T_{ins} is smaller than E_F , $\mu_e = -0.48T_{ins}$ and $\mu_e \approx E_F \gg T_{ins}$ (see Eq.(28)). Then $\tilde{\Pi}_e = O(1)$, while $\tilde{\Pi}_h \approx \log(1.13E_F/T_{ins}) \gg 1$ In this situation, $\Pi_e \Pi_h - \Pi^2 \approx \Pi \tilde{\Pi}_h$. Substituting this into Eq. (101) we obtain that, up to an overall factor,

$$T_{ins} = E_F e^{-\frac{1 + \sqrt{1 + a_{12}^2 \Pi^2}}{2a_{he}^2 \Pi}} \quad (105)$$

This is the transcendental equation on T_{ins} with temperature dependence in the r.h.s. coming from $\Pi = \log 1.13\Lambda/T_{ins}$ and from $a_{he} = a_{he}(T)$. The latter again should be treated as input parameter, extracted from independent measurements.

It is straightforward to verify that T_{ins} in Eq.(105) is the same as we obtained in Eq. (31) earlier in terms of the coupling λ (or, equivalently, in terms of E_0). To see this, we re-express a_{he} back in terms of λ . This converts Eq. (105) into

$$T_{ins} = E_F e^{-\frac{4(1 - \frac{\lambda^2 \Pi^2}{4})}{\lambda^2 \Pi}} = E_F e^{-\frac{4}{\lambda^2 \Pi}} \frac{\Lambda}{T_{ins}} \quad (106)$$

hence, up to constant prefactors,

$$\log \frac{(\Lambda E_F)^{1/2}}{T} \log \frac{\Lambda}{T} = \frac{2}{\lambda^2} \quad (107)$$

Using $\log \Lambda = (2/\lambda) + \log E_0$ we obtain after simple algebra, $T_{ins} \sim E_F^{1/3} E_0^{2/3}$, what agrees with Eq.(31).

In the opposite limit $E_0 > E_F$, we use the fact that $T_{ins} \gg E_F$, $\mu_e \approx -E_F/2$, $\mu_h \approx 3E_F/2$, and obtain $\tilde{\Pi}_e \approx -E_F/(4T_{ins})$ and $\tilde{\Pi}_h \approx 3E_F/(4T_{ins})$. Substituting into Eq.(101) and using the fact that $\Pi \gg 1$, while $\tilde{\Pi}_{e,h}$ are small, we obtain

$$T_{ins} = \frac{E_F}{2} \frac{2a_{he}^2 \Pi}{1 + \sqrt{1 + 4a_{he}^2 \Pi^2}} \quad (108)$$

Using next the fact that at small E_F , T_{ins} is close to T_0 at which the scattering amplitude diverges, i.e, $a_{he} \Pi \gg 1$, we can further approximate Eq.(108) to

$$T_{ins} = E_F \frac{a_{he}}{2} \quad (109)$$

Note that in the two-band case a_{he} remains positive (like U) for arbitrary E_F/E_0 because even at $E_F \rightarrow 0$, T_{ins} is larger than T_0 , see (41).

Eq. (109) expresses T_{ins} at $E_F \ll E_0$ in terms of E_F and 2D inter-band scattering amplitude, which, again, should be considered as temperature dependent input function.

One can easily demonstrate that Eq. (109) coincides with Eq.(41). For this we note that, when a_{he} is large, it can be expressed via the coupling λ (or, equivalently, via E_0) as

$$a_{he} \approx \frac{1}{2 \log b}, \quad (110)$$

where $b \log b \approx (E_F/4E_0)$. For small E_F/E_0 , $\log b \approx E_F/4E_0$, hence $a_{he} \approx 2E_0/E_F$. Substituting this into Eq. (109), we obtain $T_{ins} \approx E_0$. This coincides with Eq.(41) up to corrections which we neglected by approximating a_{he} by $2E_0/E_F$.

VI. CONCLUSIONS

In this paper we considered the interplay between superconductivity and formation of bound pairs of fermions in multi-band 2D fermionic systems (BCS-BEC crossover). In two spatial dimensions a bound state develops already at weak coupling, and BCS-BEC crossover can be analyzed already at weak coupling, when calculations are fully under control. We reviewed the situation in one-band model and considered two different two-band models, one with one hole and one electron band and the other with two hole or two electron bands. The first model is relevant to experiments on Fe-pnictides and Fe-chalcogenides, particularly on FeSe, the second one is used to describe Nb-doped SrTiO₃.

For each model we solved self-consistently the equations for the gaps and the chemical potentials on the two bands and obtained the onset temperature of the pairing, T_{ins} , and the chemical potentials and the pairing gaps below T_{ins} . We computed superfluid stiffnesses and used them to estimate the actual superconducting T_c below which $U(1)$ gauge symmetry is spontaneously broken.

In a one-band model, the system displays BCS behavior when the Fermi energy E_F exceeds the energy, E_0 , of a bound state of two fermions in a vacuum. In this regime, (i) $T_{ins} \sim (E_F E_0)^{1/2}$ is parametrically larger than E_0 , i.e., the pairing emerges at a much higher T than would be the temperature for the bound state formation in a vacuum, and (ii) the superfluid stiffness $\rho_s = E_F/(4\pi)$ is parametrically larger than T_{ins} , hence phase fluctuations are costly near T_{ins} . As the consequence, phase coherence sets in almost immediately after bound pairs form. In the opposite limit $E_0 \gg E_F$, the pairing develops at $T_{ins} \gg E_F$, while the actual T_c is determined by phase fluctuations and is of order E_F . In between T_{ins} and T_c bound pairs develop but remain incoherent, and the fermionic spectral function displays a pseudogap behavior, when the spectral weight gradually transforms from zero energy to an energy of order of the pairing gap $\Delta \sim (E_F E_0)^{1/2}$. This is a typical system behavior in the BEC regime. The only difference with the "canonical" BEC behavior in 3D, where strong coupling is a must, is that in our weak coupling model bound pairs are not tightly bound molecules because the two fermions in a pair are separated on average at distances by a distance well above the interatomic spacing. We argued that the fermionic spectral function is highly non-symmetric in the preformed pairs regime.

We next considered the two-band model with one hole and one electron band. For definiteness we set $E_F = 0$ on the electron band, but kept E_F finite on the hole band. We found that the behavior of this model is different in several aspects from that in the one-band model. There is again a crossover from BCS-like behavior at $E_F \gg E_0$ to BEC-like behavior at $E_F \ll E_0$ with $T_{ins} > T_c$. However, in distinction to the one-band case, the actual T_c , below which long-range superconducting order develops, remains finite and of order T_{ins} even when $E_F = 0$ on

both bands. The reason for a finite T_c is that the filled hole band acts as a reservoir of fermions. The pairing reconstructs fermionic dispersion and transforms some spectral weight into the newly created hole band below the original electron band and electron band above the original hole band. A finite density of fermions in these two bands gives rise to a finite T_c even when the bare Fermi level is exactly at the bottom of the electron band and at the top of the hole band.

We also considered the model with two hole/two electron bands. We found that the behavior in this model is similar to that in the one-band model. Namely, BCS-BEC crossover occurs when the largest of the two E_F 's becomes comparable to E_0 . When the ratio E_F/E_0 is large, the system displays BCS-like behavior, when it is small, the system displays the same BEC-type behavior as in the one-band model, namely T_c scales with E_F and is parametrically smaller than T_{ins} .

Finally, we re-expressed T_{ins} in terms of the 2D scattering amplitude, which is a physical observable, in distinction to U . For this, we extended to $D = 2$ the approach put forward by Gorkov and Melik Barkhudarov back in 1961 for $D = 3$ case. We obtained the explicit formulas for T_{ins} in terms of the 2D dimensionless scattering amplitude a_2 for the one-band model and for the model with one hole and one electron band, and demonstrated that these formulas are valid not only in the BCS limit but also in the BEC limit, when the scattering amplitude is not small. One distinction between 2D and 3D cases is that in our 2D case the scattering amplitude $a_2(T)$ is temperature dependent, hence the formulas relating T_{ins} and $a_2(T_{ins})$ are transcendental equations, which have to be solved with $a_2(T)$ taken from a separate measurement.

Our results confirm earlier BCS analysis by several groups^{8,30} that in the one hole/one electron band model T_c doesn't tend to zero if E_F on one band vanishes, and it remains finite even when one of the bands is located entirely below or entirely above the Fermi level. However, previous works identified T_{ins} with T_c , while we show that $T_c \approx T_{ins}$ only when $E_F \gg E_0$, while at $E_F < E_0$ T_c is numerically substantially smaller than T_{ins} . Our results for T_{ins} also differ from these earlier works because they neglected the temperature dependence of the chemical potential.

We summarize our results for all three models in Fig. 2 and in Table I. Our results show that the case of one hole and one electron pocket is the "best case" scenario for higher superconducting T_c at small E_F , because for this case phase fluctuations do not reduce T_c more than by a numerical factor. For a system with a single hole or electron band and for a system with two hole or two electron bands, phase fluctuations reduce T_c parametrically compared to the onset temperature of pair formation.

With respect to applications to Fe-based superconductors, our results do confirm that T_c does not vanish when one of hole bands sinks below the Fermi level or moves as a whole above the Fermi level. Furthermore, the gap on this band is generally higher than that on the

bands which cross the Fermi level. The gap ratio is non-universal and depends on the mass ratio and/or presence of additional bands. That the gap is larger on the band that does not cross the Fermi level is consistent with the experimental results reported for $\text{LiFe}_{1-x}\text{Co}_x\text{As}$ in Ref.³ and for $\text{FeTe}_{0.6}\text{Se}_{0.4}$ in Ref.⁴. We note in passing that one does not need to invoke a highly unconventional concept of the ultra-strong pairing at all momenta in the Brillouin zone³ to explain the data.

Our analysis for the case $E_F \leq E_0$ may be relevant to FeSe. In this material Fermi energies on all bands are only a few meV , and are comparable to T_c . For the two-band model, we found that T_{ins} and T_c do differ by a sizable factor, and there exists an intermediate T range of preformed pair behavior. Recent experiments on FeSe have been interpreted⁵⁰ in terms of pre-formed pairs which appear at about twice T_c . This is exciting possibility and the theoretical study of the interplay between T_{ins} and T_c in the full multi-band model for FeSe is clearly called for.

Finally, our analysis of the model with two electron pockets one of which has a finite E_F and for the other the Fermi level is near its bottom, may be relevant to superconductivity in Nb-doped SrTiO_3 (Refs.^{22,23,31,32}) and $\text{LaAlO}_3/\text{SrTiO}_3$ heterostructures (Ref. [33]). These materials contain two electron bands, and the Fermi level passes through the bottom of one of the bands upon doping. Experiments have found^{32,33} that T_c rapidly increases once the chemical potential moves up and crosses both bands. We reproduced this result in our theory – we found that T_c increases when the chemical potential moves into the second band, and the slope of the increase of T_c contains a large parameter. We, however, didn't find a jump in T_c at a critical doping, as some other experiments suggest³⁴.

We acknowledge with thanks the discussions with C. Batista, S. Borisenko, A. Charnukha, L.P. Gorkov, M. Grilli, R. Fernandes, P. Hirschfeld, C.A.R. Sa de Melo, S. Maiti, D. Mozursky, Y. Matsuda, I. Mazin, T. Shibauchi, A. Varlamov, and, particularly, with L. Benfatto and M. Randeria. We thank L. Benfatto for pointing out errors in the earlier version of the manuscript. The work was supported by the Office of Basic Energy Sciences U. S. Department of Energy under award DE-SC0014402 (AVC). The work of IE was supported by the Focus Program 1458 Eisen-Pniktide of the DFG and by the German Academic Exchange Service (DAAD PPP USA no. 57051534). AVC acknowledges with thanks support by LANL through Ulam fellowship.

VII. APPENDIX

In this Appendix we obtain the exact prefactor for T_{ins} in Eqs. (4) and (5). To compute it, one needs to go beyond ladder approximation and include the fermionic self-energy to order λ and the corrections to U from the particle-hole channel.

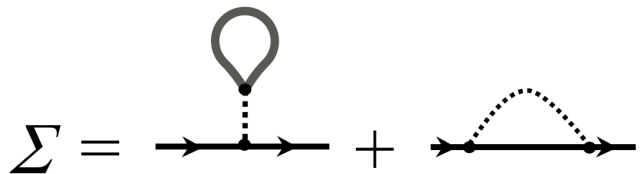


FIG. 15: Hartree-Fock diagrams for the self-energy.

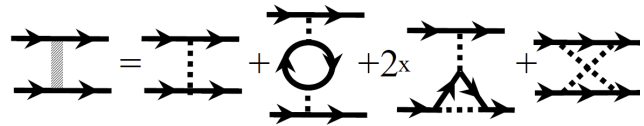


FIG. 16: Second order diagrams for the renormalization of the irreducible pairing interaction due to contributions from the particle-hole channel.

The fermionic self-energy to order λ comes from Hartree and Fock diagrams in Fig. 15. This self-energy renormalizes fermionic dispersion and the chemical potential, and also changes fermionic residue to $Z < 1$. The correction to Z originates from frequency-dependent part of the fermionic self-energy $\Sigma(k, \omega)$. The latter is non-zero in our model, despite that the interaction is approximated by the static U , because we set the sharp frequency cutoff at energy scale Λ (and momentum cutoff at $\varepsilon_k = \Lambda$).

We assume that the renormalization of μ at $T = 0$ is already incorporated into E_F . The remaining one-loop self-energy has the form

$$\Sigma(k, \omega) = i\omega \frac{\lambda}{4} f_\omega \left(\frac{\omega}{\Lambda}, \frac{\varepsilon_k}{\Lambda} \right) - \varepsilon_k \frac{\lambda}{2\pi} f_\varepsilon \left(\frac{\omega}{\Lambda}, \frac{\varepsilon_k}{\Lambda} \right), \quad (111)$$

where the scaling functions satisfy $f_\omega(0, 0) = f_\varepsilon(0, 0) = 1$. We define the sign of the self-energy via $G^{-1}(k, \omega) = i\omega - \varepsilon_k + \Sigma(k, \omega)$. The self-energy comes from internal frequency and momentum of order of the upper cutoff and only weakly depends on $E_F \ll \Lambda$. The scaling functions f_ω and f_ε can be straightforwardly obtained numerically. However, for our purposes we will need the renormalization of the fermionic propagator only at $\omega \sim \varepsilon_k \sim T_{ins} \ll \Lambda$. At these energies the scaling functions can be approximated by their values at $\omega = \varepsilon_k = 0$. The full Green function to order λ in this energy/momentum range is then

$$G(k, \omega) = \frac{Z}{\omega - \left(\frac{k^2}{2m^*} - E_F \right)}, \quad (112)$$

where

$$Z = 1 - \frac{\lambda}{4}, \quad m^* = m \left(1 + \frac{\lambda}{4} - \frac{\lambda}{2\pi} \right) \quad (113)$$

Substituting the Green's function from (112) into the ladder diagrams, we immediately obtain that the

fermionic self-energy changes the dimensionless coupling λ into

$$\tilde{\lambda} = \lambda m^* Z^2 = \lambda \left(1 - \lambda \frac{\pi + 2}{4\pi} \right) \quad (114)$$

The renormalization of the irreducible pairing interaction to order λ comes from particle-hole channel and generally involves four diagrams, each contains a particle-hole bubble (Fig. 16). For a constant interaction U the first three diagrams in Fig. 6 cancel out and only the last, exchange diagram contributes. In 2D the contribution from this diagram to the irreducible coupling (i.e., the correction to U) is a constant, equal to $U\lambda$, when relevant transferred frequency is much smaller than E_F . At a higher frequency Ω the renormalization from the exchange diagram is additionally reduced by E_F/Ω . Accordingly, the renormalization of U by the particle-hole bubble is only relevant at $E_F \gg E_0$, when $T_{ins} \ll E_F$. In this regime, the effective coupling constant is

$$\lambda_{eff} = \tilde{\lambda}(1 - \lambda) = \lambda \left(1 - \lambda \frac{5\pi + 2}{4\pi} \right) \quad (115)$$

In the opposite limit, $E_F \ll E_0$, $T_{ins} \gg E_F$, and the renormalization from particle-hole channel can be neglected. In this regime, the effective coupling is

$$\lambda_{eff} = \tilde{\lambda} = \lambda \left(1 - \lambda \frac{\pi + 2}{4\pi} \right) \quad (116)$$

Collecting all renormalizations to order λ and substituting into Eqs. (4) and (5), we obtain for T_{ins} at $E_F \gg E_0$,

$$T_{ins} = 1.13(\Lambda E_F)^{1/2} e^{-1/\tilde{\lambda}} = 0.276(\Lambda E_F)^{1/2} e^{-1/\lambda} \quad (117)$$

The prefactor differs somewhat from that in Ref. [35b]. At $E_F \ll E_0$ we have

$$T_{ins} = 1.13 \frac{\Lambda}{\log E_0/E_F} e^{-2/\tilde{\lambda}} = 0.751 \frac{E_0}{\log E_0/E_F} \quad (118)$$

-
- ¹ Y. Kamihara, T. Watanabe, M. Hirano, and H. Hosono, *J. Am. Chem. Soc.* **130**, 3296 (2008).
- ² D. C. Johnston, *Adv. Phys.*, **59**, 803 (2010); D.N. Basov and A.V. Chubukov, *Nature Physics* **7**, 241 (2011); J. Paglione and R. L. Greene, *Nature Phys.* **6**, 645 (2010); P. C. Canfield and S. L. Bud'ko, *Annu. Rev. Cond. Mat. Phys.* **1**, 27 (2010); A. Kordyuk *Low Temp. Phys.*, **38**, 888 (2010); H. H. Wen and S. Li, *Annu. Rev. Cond. Mat. Phys.* **2**, he1 (2011); G. R. Stewart, *Rev. Mod. Phys.*, **83**, 1589 (2011); P.J. Hirschfeld, M.M. Korshunov, and I.I. Mazin, *Rep. Prog. Phys.* **74**, he4508 (2011); A.V. Chubukov, *Annu. Rev. Cond. Mat. Phys.* **3**, 57 (2012); Hideo Hosono and Kazuhiko Kuroki, *Physica C: Superconductivity and its Applications* **514**, 399 (2015)
- ³ H. Miao, T. Qian, X. Shi, P. Richard, T.K. Kim, M. Hoesch, L.Y. Xing, X.-C. Wang, C.-Q. Jin, J.-P. Hu, and H. Ding, *Nature Commun.* **6**, 6056 (2015)
- ⁴ K. Okazaki, Y. Ito, Y. Ota, Y. Kotani, T. Shimojima, T. Kiss, S. Watanabe, C. T. Chen, S. Niitaka, T. Hanaguri, H. Takagi, A. Chainani, S. Shin, *Sci. Rep.* **4**, 4109, (2014).
- ⁵ A. Charnukha, S. Thirupathaiiah, V. B. Zabolotnyy, B. Bchner, N. D. Zhigadlo, B. Batlogg, A. N. Yaresko, and S. V. Borisenko, *Sci. Rep.* **5**, 10392 (2015); J. Fink, A. Charnukha, E.D.L. Rienks, Z.H. Liu, S. Thirupathaiiah, I. Avigo, F.Roth, H.S.Jeevan, P. Gegenwart, M. Roslova, I.Morozov, S. Wurmehl, U.Bovensiepen, S. Borisenko, M. Vojta, B. Buechner, arXiv:1501.02135 and references therein.
- ⁶ T. Terashima, N. Kikugawa, A. Kiswandhi, E.-S. Choi, J.S. Brooks, S. Kasahara, T. Watashige, H. Ikeda, T. Shibauchi, Y. Matsuda, Th. Wolf, A.E. Böhmer, F. Hardy, Ch. Meingast, H. v. Lhneysen, M.-T. Suzuki, R. Arita, and S. Uji, *Phys. Rev. B* **90**, 144517 (2014).
- ⁷ S. Kasahara, T. Watashige, T. Hanaguri, Y. Kohsaka, T. Yamashita, Y. Shimoyama, Y. Mizukami, R. Endo, H. Ikeda, K. Aoyama, T. Terashima, S. Uji, T. Wolff, H. von Löhneysen, T. Shibauchi, and Y. Matsuda, *PNAS* **111**, 16309 (2014).
- ⁸ X. Chen, S. Maiti, A. Linscheid, and P.J. Hirschfeld, arXiv:1508.04782 (unpublished)
- ⁹ K. Kuroki, S. Onari, R. Arita, H. Usui, Y. Tanaka, H. Kontani, and H. Aoki *Phys. Rev. Lett.* **101**, 087004 (2008).
- ¹⁰ I. I. Mazin, D. J. Singh, M. D. Johannes, and M. H. Du, *Phys. Rev. Lett.* **101**, 057003 (2008).
- ¹¹ K. Miyake, *Prog. Theor. Phys.* **69**, 1794 (1983).
- ¹² Nozieres and S. Schmitt-Rink, *J. Low Temp. Phys.* **59**, 195 (1985).
- ¹³ M. Randeria, J-M Duan, and L-Y Shieh, *Phys. Rev. Lett.* **62**, 981 (1989); *Phys. Rev. B* **41**, 327 (1990).
- ¹⁴ Y. Ohashi and A. Griffin, *Phys. Rev. A* **67**, 033603 (2003)
- ¹⁵ C.A.R. Sa de Melo, M. Randeria, and J.R. Engelbrecht, *Phys. Rev. Lett.*, **71**, 3202 (1993); J.R. Engelbrecht, M. Randeria, and C.A.R. Sa de Melo, *Phys. Rev. B* **55**, 15153 (1997).
- ¹⁶ Y. L. Loh, M. Randeria, N. Trivedi, C-C. Chang, and R. Scalettar, arXiv:1507.05641
- ¹⁷ V. B. Geshkenbein, L. B. Ioffe, and A. I. Larkin, *Phys. Rev. B* **55**, 3173 (1997).
- ¹⁸ B. Tobijasewska and R. Micnas, *Acta Physica Polonica A* **97**, 393 (2000).
- ¹⁹ L. Benfatto, A. Toschi, S. Caprara, and C. Castellani, *Phys. Rev. B* **64**, 140506(R) (2001); L. Benfatto, S. Caprara, C. Castellani, A. Paramekanti, and M. Randeria, *Phys. Rev. B* **63**, 174513 (2001); L. Benfatto, A. Toschi, and S. Caprara, *Phys. Rev. B* **69**, 184510 (2004).
- ²⁰ M. Iskin and C.A.R. Sa de Melo, *Phys. Rev. B* **74**, 144517 (2006).
- ²¹ L. Fanfarillo, L. Benfatto, S. Caprara, C. Castellani, and M. Grilli, *Phys. Rev. B* **79**, 172508 (2009).
- ²² D. Innocenti, N. Poccia, A. Ricci, A. Valletta, S. Caprara, A. Perali, and A. Bianconi, *Phys. Rev. B* **82**, 184528 (2010).

- ²³ A. Bianconi, D. Innocenti, A. Valletta, and A. Perali, *J. of Phys.: Conf. Ser.* **529**, 012007 (2014).
- ²⁴ A. Levchenko, M. R. Norman, and A. A. Varlamov, *Phys. Rev. B* **83**, 020506(R) (2011).
- ²⁵ L. Fanfarillo, L. Benfatto, and C. Castellani, *Phys. Rev. B* **85**, 024507 (2012).
- ²⁶ A. Guidini and A. Perali, *Supercond. Sci. Technol.* **27**, 124002 (2014).
- ²⁷ see M. Y. Kagan, "Modern Trends in Superconductivity and Superfluidity" *Lecture Notes in Physics*, 874, Springer, Heidelberg/Germany (2013) and references therein.
- ²⁸ Q. Chen, J. Stajic, S. Tan, and K. Levin, *Phys. Rep.* **412** 188 (2005); Y. Shin, C.H. Schunck, A. Schirotzek, A. and W. Ketterle, *Nature* **451** 689693 (2007); S. Giorgini, L.P. Pitaevskii, and S. Stringari, *Rev Mod Phys* **80**, 1215 (2008); F. Chevy and C. Mora, *Rep. Prog. Phys.* **73**, 112401 (2010); Z. Shen, L. Radzihovsky, and V. Gurarie, *Phys. Rev. Lett.* **109**, 245302 (2012); M. Randeria and E. Taylor, *Ann. Rev. Condens. Matter Phys.* **5** 209232 (2014).
- ²⁹ J.P. Gaebler *et al*, *Nature Physics*, **6**, 569 (2010).
- ³⁰ Z. Leong, and P. Phillips, arXiv:1506.04762 (unpublished).
- ³¹ R. M. Fernandes, J. T. Haraldsen, P. Wölfle, and A. V. Balatsky *Phys. Rev. B* **87**, 014510 (2013).
- ³² see D. van der Marel, J.L.M. van Mechelen, and I.I. Mazin, *Phys. Rev. B* **84**, 205111 (2011) and references therein
- ³³ A. Joshua, S. Pecker, J. Ruhman, E. Altman, and S. Ilani, *Nat. Commun.* **3**, 1129 (2012).
- ³⁴ J. Biscaras *et al*, *Phys. Rev. Lett.* **108**, 247005 (2012).
- ³⁵ (a) L.P. Gorkov, T.K. Melik-Barkhudarov, *Jour. Exp. Teor. Fiz.* **40**, 1452 (1961) [*Soviet Physics JETP* **13**, 1081 (1961)]. (b) This approach has been recently reviewed in L.P. Gorkov, arXiv:1509.08488 (unpublished).
- ³⁶ For extension of the GMB approach to p-wave and d-wave superconductivity see, respectively, A. V. Chubukov and A. Sokol *Phys. Rev. B* **49**, 678 (1994) and Y. Wang and A. V. Chubukov *Phys. Rev. B* **88**, 024516 (2013).
- ³⁷ L.D. Landau, and E.M. Lifshitz, *Statistical Physics*, Vol.2, (Pergamon Press, 1980).
- ³⁸ Anatoly Larkin and Andrei Varlamov, "Theory of fluctuations in superconductors" OUP Oxford, 2005.
- ³⁹ N. Nagaosa, "Quantum field theory in condensed matter", Springer, 1999.
- ⁴⁰ See e.g., V.L. Pokrovsky, *Advances in Physics* **28**, 595 (1979).
- ⁴¹ M.R. Beasley, J.E. Mooij, and T.P. Orlando, *Phys. Rev. Lett.* **42**, 1165 (1979).
- ⁴² D.J. Scalapino, S.R. White, and S. Zhang, *Phys. Rev. B* **47**, 7995 (1993).
- ⁴³ The authors are thankful to M. Randeria for clarifying this issue.
- ⁴⁴ V.N. Popov, *Theor. Math. Phys.* **11**, 565 (1972); D.S. Fisher and P.C. Hohenberg, *Phys. Rev. B* **37**, 4936 (1988).
- ⁴⁵ L. Benfatto, private communication
- ⁴⁶ S.G. Sharapov, V.P. Gusynin, and H. Beck, *Eur. Phys. J. B* **30**, 45 (2002).
- ⁴⁷ R. M. Fernandes, A. V. Chubukov, J. Knolle, I. Eremin, and J. Schmalian *Phys. Rev. B* **85**, 024534 (2012).
- ⁴⁸ Y. Wang and A.V. Chubukov *Phys. Rev. B* **90**, 035149 (2014).
- ⁴⁹ A.A. Abrikosov, L.P. Gorkov, and I.E. Dzyaloshinskii, *Methods of quantum field theory in statistical physics*, (Pergamon Press, 1965)
- ⁵⁰ S. Kasahara, T. Watashige, T. Hanaguri, Y. Kohsaka, T. Yamashita, Y. Shimoyama, Y. Mizukami, R. Endo, H. Ikeda, K. Aoyama, T. Terashima, S. Uji, T. Wolf, H. v. Lhneysenn, T. Shibauchi, Y. Matsuda, *PNAS* **111**, 16309 (2014).
- ⁵¹ S. Maiti, M. Sigrist, and A.V. Chubukov, *Phys. Rev. B* **91**, 161102 (2015).
- ⁵² A. Perali, C. Castellani, C. Di Castro, M. Grilli, E. Piegari, and A. A. Varlamov, *Phys. Rev. B* **62**, 9295 (2000).